Author/s:
Chapman, M;Rajagopal, V;Stewart, A;Collins, DJ

Title:
Critical review of single-cell mechanotyping approaches for biomedical applications

Date:
2024

Citation:
Chapman, M., Rajagopal, V., Stewart, A. & Collins, D. J. (2024). Critical review of single-cell mechanotyping approaches for biomedical applications. Lab on a Chip, 24 (12), pp.3036-3063. https://doi.org/10.1039/d3lc00978e.

Persistent Link:
https://hdl.handle.net/11343/345637

Critical review of single-cell mechanotyping approaches for biomedical applications

Max Chapman[1], Vijay Rajagopal[1], Alastair Stewart[2,3] & David Collins[1]

[1]Department of Biomedical Engineering, University of Melbourne, Melbourne, Victoria, Australia
[2]ARC Centre for Personalised Therapeutics Technologies, The University of Melbourne, Parkville, VIC, Australia
[3]Department of Biochemistry and Pharmacology, The University of Melbourne, Parkville, VIC, Australia

Abstract

Accurate mechanical measurements of cells has the potential to improve diagnostics, therapeutics and advance understanding of disease mechanisms, where high-resolution mechanical information can be measured by deforming individual cells. Here we evaluate recently developed techniques for measuring cell-scale stiffness properties; while many such techniques have been developed, much of the work examining single-cell stiffness is impacted by difficulties in standardization and comparability, giving rise to large variations in reported mechanical moduli. We highlight the role of underlying mechanical theories driving this variability, and note opportunities to develop novel mechanotyping devices and theoretical models that facilitate convenient and accurate mechanical characterisation. Moreover, many high-throughput approaches are confounded by factors including cell size, surface friction, natural population heterogeneity and convolution of elastic and viscous contributions to cell deformability. We nevertheless identify key approaches based on deformability cytometry as a promising direction for further development, where both high-throughput and accurate single-cell resolutions can be realized.

Keywords: mechanotyping, high throughput, mechanobiology, cell mechanics, biomechanics, etc.

Introduction

Mechanotyping describes the characterization of cellular mechanical phenotypes. While technologies exist for measuring cell volume[1] and mass properties,[2] more recent work seeks to introduce single-cell stiffness as a mechanical biomarker.[3] Such work has linked changes in cell stiffness to a range of pathological conditions including cancer development,[4–8] diabetes mellitus,[9,10] malarial infection,[11–13] haemolytic disorders[14–17] and age/lifestyle factors.[9,18] In these contexts, stiffness-based cellular mechanotyping can be exploited to study disease mechanisms and responses to therapeutics[6,14,19] or for diagnosis.[20] Unlike many traditional cell analysis techniques such as fluorescence-activated cell sorting or histopathological tissue analysis, stiffness-based mechanotyping does not require biochemical labels, bringing benefits in simplified cell preparation and reduced labour.[21] Additionally, mechanotyping yields

information that is not directly measurable via optical methods alone, permitting the analysis of biological processes that do not present visual markers.[20] Recent developments in microfluidic techniques have enabled high-throughput mechanotyping approaches that are particularly useful for screening and diagnostic assessments.[21–23] Such systems have demonstrated compatibility with liquid biopsies,[6,13] and are less reliant on human interpretation than histopathological analysis.[21] These characteristics support cell mechanotyping as a non-invasive clinical screening tool, with decreased need for clinical expertise to interpret data and improved reliability. Mechanotyping advancements would accordingly benefit the treatment of diseases such as cancer, for which early-stage diagnosis is a critical factor in patient outcomes.[22–24]

In typical mechanical analysis, stiffness measurements require the application of a known force and observation of the resulting sample deformation. Material stiffness may then be calculated by relating the force and displacement data using an appropriate theoretical model, which in the case of cells requires assumptions or approximations of the cell geometry and the mechanical probe or non-contact force field. In the case of single-cell mechanotyping, applying controlled forces on microscale objects presents a significant engineering challenge, due primarily to difficulties in the fabrication of mechanical systems at cellular length scales. Several approaches have been implemented that seek to apply forces on cells via mechanical probes, hydrodynamic/hydrostatic stresses, and magnetic, optical, electric or acoustic fields. One microscale technique for deforming cells adhered to substrates is indentation by microscale cantilever-mounted probes, including commercially available Atomic Force Microscopy (AFM) devices,[6,18,25,26] parallel-plate devices and "cytoindenter" devices.[27–29] Another method for analysing adherent cells involves magnetic manipulation of ferromagnetic microparticles to apply twisting forces to the cell membrane.[30–32] Meanwhile, a variety of mechanisms have also been applied to deform cells in fluid suspensions. Optical radiation pressure is widely used to stretch soft cells, both by displacing adhered microbeads[14] and by exerting optical forces directly on the cell surface.[5,7,33] A variety of micropipette[34–36] and microfluidic devices[37–39] can further apply deforming forces to cells via contact with constriction walls, or in some cases, by hydrodynamic fluid shear forces.[40–43] Individual cells may also be trapped and stretched between a pair of electrodes by exploiting the dielectrophoretic interaction between the cell membrane and an electric field.[44–48] Lastly, a developing range of microfluidic devices have applied deforming or displacing forces on suspended cells by exploiting the differential interaction between acoustic waves and cells or media. These "acoustofluidic" devices create time-averaged acoustic force fields around cells or lipid vesicles, either by exciting bulk resonance in microfluidic channels,[49–51] or generating surface acoustic waves (SAWs) along the substrate surface.[52]

Force and displacement data alone do not fully characterize sample stiffness, however, as the manner in which the force is applied and the sample's material composition and shape, all of which are complex and nonuniform in cells, contribute to the result.[35,53,54] Some mechanotyping approaches therefore do not yield absolute stiffness measurements, instead utilizing differences in observed deformation benchmarked against the population mean to study a cell sample.[13,37–41,55] This approach has advantages of reduced computational expense

and generally enables high experimental throughput.[40,56,57] The opportunity for translation of results between different laboratories, experimental setups or cell types, however, is limited due to the absence of well-characterized and standardised samples. Alternative methods, however, apply a theoretical mechanical model of a cell to experimental observations, allowing an absolute metric of cell stiffness to be estimated.[6,25,27,31,34,58–63] While terminology relating to the mechanical properties of cells is sometimes applied inconsistently, the terms "stiffness" or "elasticity" are generally used when describing a calibrated stress-strain response, characterised by a mechanical modulus. Meanwhile, the term "deformability" is usually used where a theoretical model is not applied to experimental results and only a comparative measure of cell deformation is reported. For consistency, we follow this convention here.

Determining a stiffness value from experimental data thus requires the application of an appropriate mathematical model that relates applied stress to resulting strain. The majority of studies reporting absolute cell stiffness values employ solid elastic[6,25,31,64] or Newtonian liquid drop[34,35] models to approximate cell behaviour. Solid elastic models are generally applied to stiff cells such as epithelial cells[25] or chondrocytes,[65] or where strains are otherwise comparatively small.[35] In these cases, stiffness is quantified using elastic moduli (Young's modulus E, shear Modulus G or bulk modulus K). Common solid elastic models include the Hertz model,[66] widely used to approximate the probe-cell interaction in cantilever indentation mechanotyping, and the elastic half-space model that describes the partial aspiration of elastic cells.[58] Soft cells, for example red blood cells or neutrophils**,** are instead often analysed using the Newtonian liquid drop model, in which the cell is treated as an incompressible liquid core surrounded by an infinitesimal membrane with tensile stiffness. Here dynamic cell stiffness is quantified using cortical tension (β) and viscosity (μ).[34,35] When applying more complex analyses such as viscoelastic[61,67], power-law structural damping[68–70] or non-Newtonian liquid drop[71] models, additional material constants are required to capture cellular mechanical behaviour. For a more detailed evaluation of these models, the reader is encouraged to consult reviews by Lim et al.[54] and Rajagopal et al.[72]

Whereas previous reviews have examined the historical[21] and clinical[20] application of mechanotyping or focussed on specific subsets of mechanotyping technology,[73,74] here we present a summary of state-of-the art single-cell mechanotyping technologies with emphasis on the fundamental physical process governing each device's function, and the limitations associated with each approach. We further highlight the role of mathematical modelling in estimating intrinsic cellular properties, including cases where generalised or simplified theory limits the accuracy of results. In doing so we highlight developing approaches that combine low fabrication cost, microfluidic cell handling and the ability to modulate deforming forces,[52,75] in addition to recent developments supporting the potential for machine learning to enhance characterization[76–80] We also identify directions for future work to improve the throughput, data quality and reliability of single-cell mechanotyping measurements.

Single-cell stiffness as a biomarker for disease

Cells experience a variety of mechanical forces from their environment due to intercellular adhesion, the extracellular matrix and hydrodynamic forces.[81] The mechanical properties of cells play an important role in defining their function within healthy bodies and for a range of disease states.[82,83] Conversely, changes to the cytoskeleton or cell membrane due to pathological factors result in altered shape and mechanical properties of individual cells. An example of this interplay occurs in red blood cells, which during normal function are round and highly deformable, enabling traversal through narrow constrictions in blood vessels. In sickle cell disease, however, an inherited genetic mutation results in the development of stiff fibres in the cytoskeleton, resulting in sickle-shaped red blood cells with increased rigidity.[16] These sickle-cells have poor deformability, limiting passage through capillaries and causing blockages in the vascular network, resulting in ischemia.[15,16] Increased red blood cell stiffness has also been observed during malarial infection[13,19] and in patients with diabetes mellitus[9,10] or a history of smoking.[9] Similar relationships between pathological development and mechanical phenotype exist for a range of cell types and diseases. Reduced cell stiffness has been observed in metastatic cancer cells taken from lung, breast and pancreatic cancers, which are greater than 70% softer than healthy cells.[84] Remmerbach et al. similarly found a 3.5-fold reduction in stiffness for oral squamous carcinoma cells compared to benign cells.[7] This reduction in cellular stiffness may be a critical factor in the migration of tumours to new sites, as softer cells are better suited to traverse vessels during extravasation and intravasation.[21,85–87] A notable exception to this trend is in leukemia, where leukemic cells display higher stiffness than normal leukocytes. In this case, reduced deformability of tumour cells inhibits motility, which is suggested as a potential mechanism for leukostasis.[26]

In some cases, mechanical alterations at the single-cell level occur with sufficient frequency to produce observable changes in large cell populations.[13] Here approaches such as cell monolayer rheology[88] can be used to measure bulk properties of multicellular samples. However, other disease events may be marked by cellular mechanical changes in only a small sub-population. Despite comprising only a small proportion of the population of a pleural or blood sample, for instance, the presence of metastatic cancer cells has dramatic consequences for diagnosis and treatment.[89] Identification of these cells via stiffness measurements is possible using single-cell analysis,[84] whereas in bulk measurements population heterogeneity and extracellular composition often mask changes in single-cell behaviour.[20] Figure 1 compares hypothetical single-cell and bulk mechanotyping results, showing the improved ability to identify an enhanced subpopulation when utilizing single-cell based approaches.

By leveraging the relationship between mechanical properties and cell function, cell stiffness is therefore a useful tool in identifying unhealthy or otherwise diseased cells.[21] This capability has extensive applications in pathophysiological research, where quantitative mechanical characterisation of these cells aids our understanding of disease mechanisms[90–92] and the responses of these cells to new drug treatments.[55,93] The ability to identify unhealthy cells rapidly and without biochemical markers also has significant implications for the potential of low-cost, non-invasive diagnostic screening procedures, where the onset of diseases such as cancer could be detected before physical symptoms present.[20]

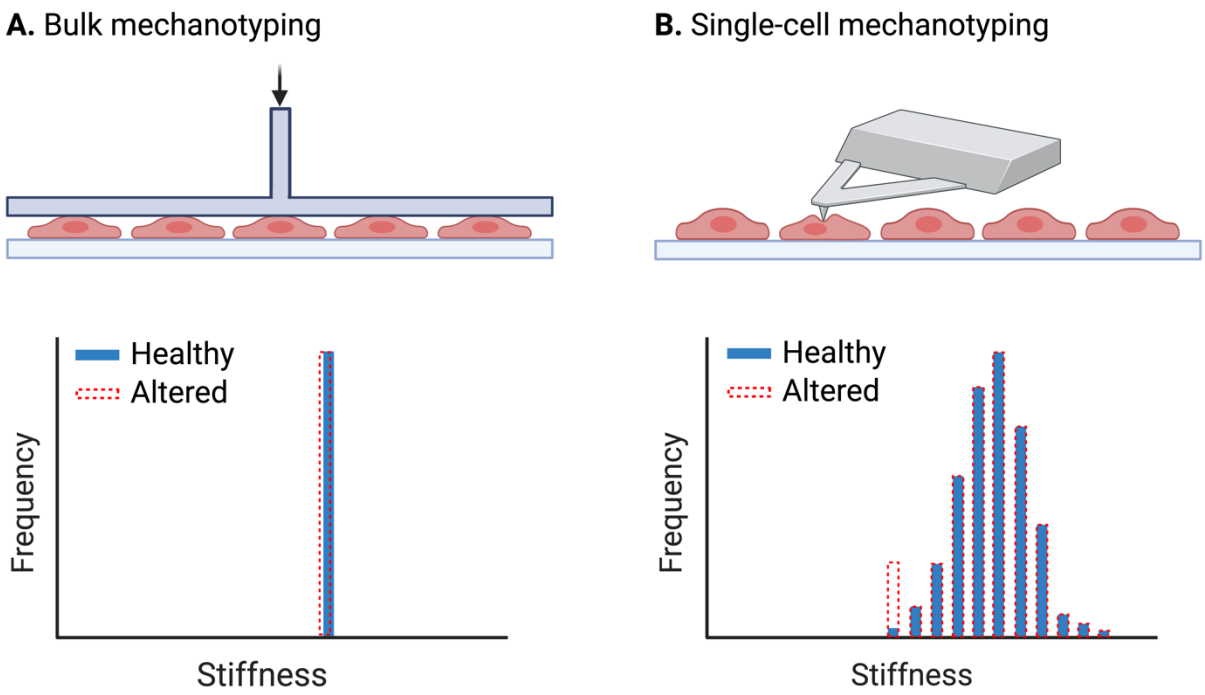

Figure 1. Comparison of single-cell and bulk mechanotyping analyses for a healthy cell population (solid blue) and diseased/altered cell population (dashed red). The altered cell population is characterised by the increased presence of low-stiffness cells. This produces a trivial change to the bulk value (a) but is easily detectable in a distribution of single-cell results (b).

Challenges

Several factors impede the accurate extraction of mechanical data from cells in large populations. One of these is the microscale dimensions of the objects being analysed. Mechanical phenotyping inherently requires the exertion of forces and observation of displacements, both of which are more difficult to reliably perform at smaller scales. Due to the small size of cells, deforming forces are typically on the order of nanonewtons and deformations are on the order of microns or smaller.[35] This necessitates high precision manipulation and observation apparatus, increasing the cost and complexity of mechanotyping systems. The general problem of calibration also challenges the accurate characterisation of elastic moduli due to the microscale dimensions of the required mechanical systems. Many standard approaches for calibrating load cells, i.e. with reference springs, cantilevers or calibrated masses, are impractical for cellular mechanotyping systems, particularly those using integrated microfluidic approaches for cell processing. Recently, a trend has emerged for using synthesised elastomer beads to calibrate the strength of deforming force fields.[43,56,94] However as these are not widely available they are usually fabricated on a case-by-case basis with significant uncertainty in stiffness values. As well as these challenges, leading non-contact methods using optical, dielectrophoretic and acoustofluidic interactions rely on physical contrast between the cell and its surrounding medium to determine the strength of deforming forces. In these cases, the forces acting on cells depends on additional biophysical properties that are intrinsic to the cell (refractive index, electrical permittivity and acoustic impedance

respectively) and cannot be directly calibrated via comparison with synthesised samples. Due to these challenges, many high throughput systems assume generic literature values to estimate cell contrast, introducing significant uncertainty to the experimental load case.

The intricate network of interactions between many structures and components inside the cell also impairs the translation of measurement data into meaningful conclusions.[95] Subcellular organisation and interactions between the cell membrane, the three classes of cytoskeletal proteins, and additional cross-linking proteins all lead to nonlinear, viscoelastic, anisotropic and heterogeneous sub-cellular mechanical properties.[54,72,96,97] The resulting mechanical properties can therefore differ substantially from the idealised models widely used to extract absolute, whole-cell scale stiffness values from mechanotyping measurements. The linear elastic Hertz model, widely used to calculate Young's modulus values from AFM measurements, is accordingly valid only for small deformations[98] and becomes increasingly inaccurate when probing away from the cell centre.[53] The elastic half-space model is also valid only for small deformations where the protruding section of the cell is approximately hemispherical during micropipette aspiration.[35] Micropipette aspiration studies have also demonstrated variation in apparent viscosity and membrane elasticity with aspiration pressure when modelling cells as liquid drops,[99,100] suggesting that simple liquid drop models with Newtonian fluid properties and linear elastic membrane stiffness do not fully capture cell stiffness behaviour. These theoretical models are discussed and compared in a later section.

The large variability of cellular mechanical stiffness values reported in literature can be attributed in part to the discrepancies between simplified analytical models and actual cell composition.[95] Complex cell structure may lead to different output stiffness measurements under different loading conditions (Fig. 2), highlighting the importance of producing multiple points of measurement across different loading conditions, as well as the utilization of models that can capture complex, non-linear stress-strain curves. Material nonlinearity produces conflicting measurements of Young's modulus at different strain magnitudes, for instance, when modelled solely in the linear elastic regime (Fig. 2a). This results from strain-softening or strain-hardening behaviour in the material and geometric considerations from the probe interface, yielding nonlinearity when probed at varying length scales and large strain magnitudes (Fig. 2b). These changes in the cell and cell-probe contact area are neglected by small-strain models such as the Hertz model. Internal and external asymmetry may also produce variation in reported stiffness with differences in orientation (Fig. 2c). Without standardised experimental loading conditions, these factors produce significant variability in stiffness results when applying idealised theory to model cell stiffness measurements.[95]

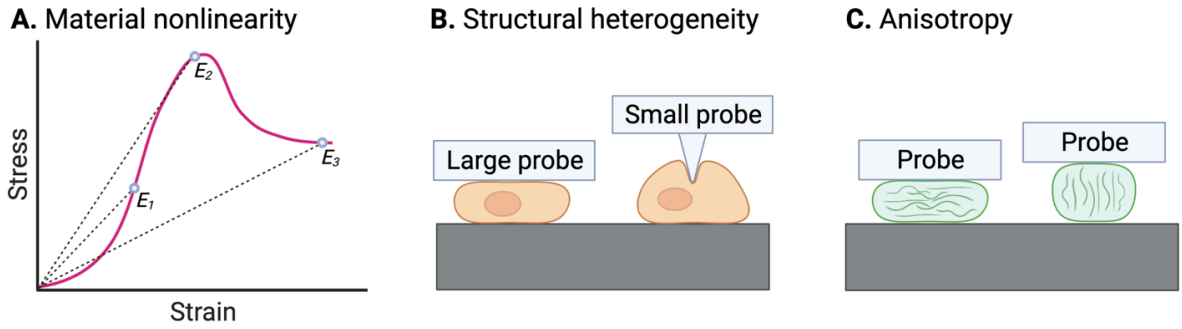

Figure 2. Schematic representations of complex cell stiffness properties across different loading conditions. (a) Example stress/strain graph showing three different elastic moduli extracted from a single nonlinear curve. (b) Alternative deformation modes under loading at different length scales due non-homogeneous internal structure and geometric nonlinearity. (c) Contrasting stiffness behaviour measured in different directions due to anisotropic makeup.

Population heterogeneity within cell samples is particularly confounding for mechanotyping applications where known mechanical biomarkers are comparatively rare. In small samples, the presence of a subpopulation with altered mechanical properties may be masked by natural variations in cell stiffness. This is especially detrimental for clinical mechanotyping applications such as the screening of tumour cells, where a metastatic subpopulation of interest may only comprise a small proportion of the sample.[89] The use of large sample sizes is therefore crucial in minimising the influence of population heterogeneity, as this enables small subpopulations to be identified from a distribution with improved statistical significance.[97] Consequently, mechanotyping systems capable of processing cell samples at high throughputs are ideal for clinical use.[20,21]

Single-cell mechanotyping techniques

Existing techniques for the mechanical characterisation of individual cells use a range of approaches for cell handling and mechanical probing. Broadly, these can be classified into two groups, namely devices that analyse cells adhered to substrates (Fig. 3a-c) and those in which cells are processed in a fluid suspension (Fig. 3d-i). These techniques are described and evaluated in the following sections.

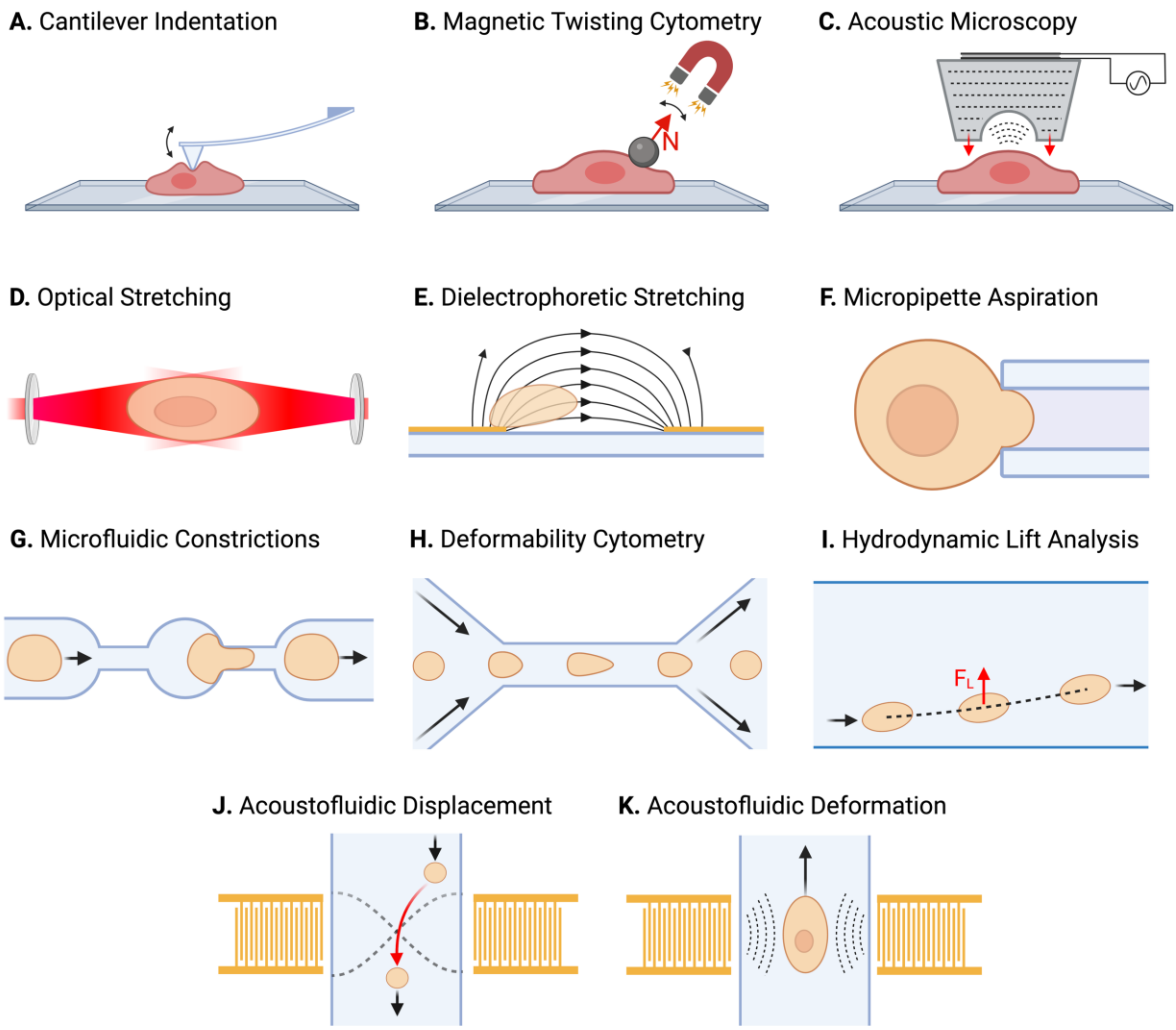

Figure 3. Schematic representations of (a-c) substrate-based and (d-k) suspension-based mechanotyping techniques.

Mechanotyping cells adhered to substrates

Cantilever Indentation

A method for accurately probing mechanophenotype on substrate-bound cells employs flexible cantilevers to deform cells and infer contact forces. These devices incorporate four fundamental components, namely a stiff substrate, a flexible cantilever and an actuation system permitting precise displacement of the cantilever base, and a sensor for the measurement of cantilever deflection. Cells adhered to the substrate are compressed by a probe mounted at the cantilever tip, causing both a local deformation in the cell and deflection of the cantilever. Meanwhile, measurements of cantilever deflection and base displacement enable calculation of indentation depth and force, which together reveal cell stiffness properties. Due to their technological maturity, commercially available Atomic Force Microscope (AFM) devices are widely used to probe cells in this manner.[6,8,9,101–103] A range of cell-specific cantilever indentation devices have also been developed, offering flexibility in the magnitude and geometry of the probing force.[27–29,95,104] AFM is also capable of achieving topographical measurements of features down to atomic scales for mechanical samples,[105] where the

remarkable precision of AFM technology is due in part to advanced cantilever deflection tracking mechanisms, which generally use laser deflection or electron tunnelling systems to detect small displacements.[106] Using cantilever stiffnesses on the order of the sample stiffness enables precise stiffness data to be extracted from across the exposed area of the cell. Cell mechanotyping-focused devices operating on AFM principles have also been developed, largely motivated by the desire for reduced apparatus cost and increased flexibility in probe geometries and deforming force magnitudes. Examples of these devices include cylindrical "cytoindenter"[27–29] (Fig. 4a) and parallel-plate[95,104] devices, which are often preferred for studying fragile cells due to their increased contact area.[107] To date, however, these devices have only been implemented with microscope-based cantilever deflection measurements, and thus offer lower measurement resolution than commercial, materials-focused AFM devices.

Cantilever-based mechanotyping has been widely implemented in biomedical applications as a means of mechanically probing cells, particularly in relation to the identification and characterisation of cancer cells.[6,8,25,84,101,102,108] Figure 4 (b) shows an ovarian cancer cell undergoing AFM indentation analysis. Mechanotyping using cantilever indentation generally has shown reduced Young's modulus with increasing malignancy and metastatic potential.[6,8,102,109] A notable exception to this trend is leukaemia, with mature leukocytes being stiffer than immature ones.[26] Cantilever-based cellular mechanotyping also has broader research implications outside of cancer analysis. The ability to vary probing force in real time enables highly detailed mechanical analysis of cellular properties, including the extraction of complex force-displacement curves.[64,103,109,110] Meanwhile, the use of different tip geometries allows stiffness to be probed at different length scales.[109] Dynamic and frequency-based AFM studies have also probed the viscoelastic behaviour of alveolar and bronchial epithelial cells[25] and mouse fibroblasts.[103,110,111] Collectively, such cantilever-based force/displacement data have informed numerous mechanical models of living cells.[64,72,98]

Automation and throughput, however, remain significant challenges for cantilever mechanotyping, limiting its application to small cell populations.[20,21] Attempts to automate probing positions across multiple cells have achieved throughputs of approximately 20 cells per minute, at which point the measurement rate is primarily limited by the indentation process.[112] While this presents a substantial improvement over manual AFM indentation, higher measurement rates are still desired for practical measurement of large cell samples.[21] Other efforts to improve the practical throughput of AFM-based mechanotyping include simultaneous indentation measurements using an array of AFM probes.[113] Due to difficulties in accurately positioning cells on a substrate, however, this method is more suitable for scanning measurements than for static indentation of cells, and thus has not meaningfully improved the throughput of AFM stiffness measurements.

Another challenge for cantilever-based mechanotyping is the isolation of cell properties from external stimuli. It is known that substrate stiffness influences stiffness measurements of adherent cells,[114–119] especially as the probe moves away from the cell centre.[53] Other confounding factors include the influence of focal adhesions,[53] ECM[97] and variation in probe tip geometry,[95] all of which can skew mechanical moduli results obtained via the prevalent

Hertz model.[66] This, consequently, impedes the extraction of generalised stiffness values that provide comparable results with other techniques. Recent work has sought to improve the scalability of cantilever indentation to analysis of free-floating cells. One method to achieve this involves the addition of microwells in the substrate to trap cells from continuous flow.[26] Commercially-available fluidFM devices, meanwhile, integrate a negative-pressure capillary in the probe to reversibly adhere free-floating cells to the probe prior to indentation.[120] Both of these approaches eliminate the influence of substrate adhesion on measured stiffness. However, they do not significantly impact the achievable throughput of cantilever indentation mechanotyping.

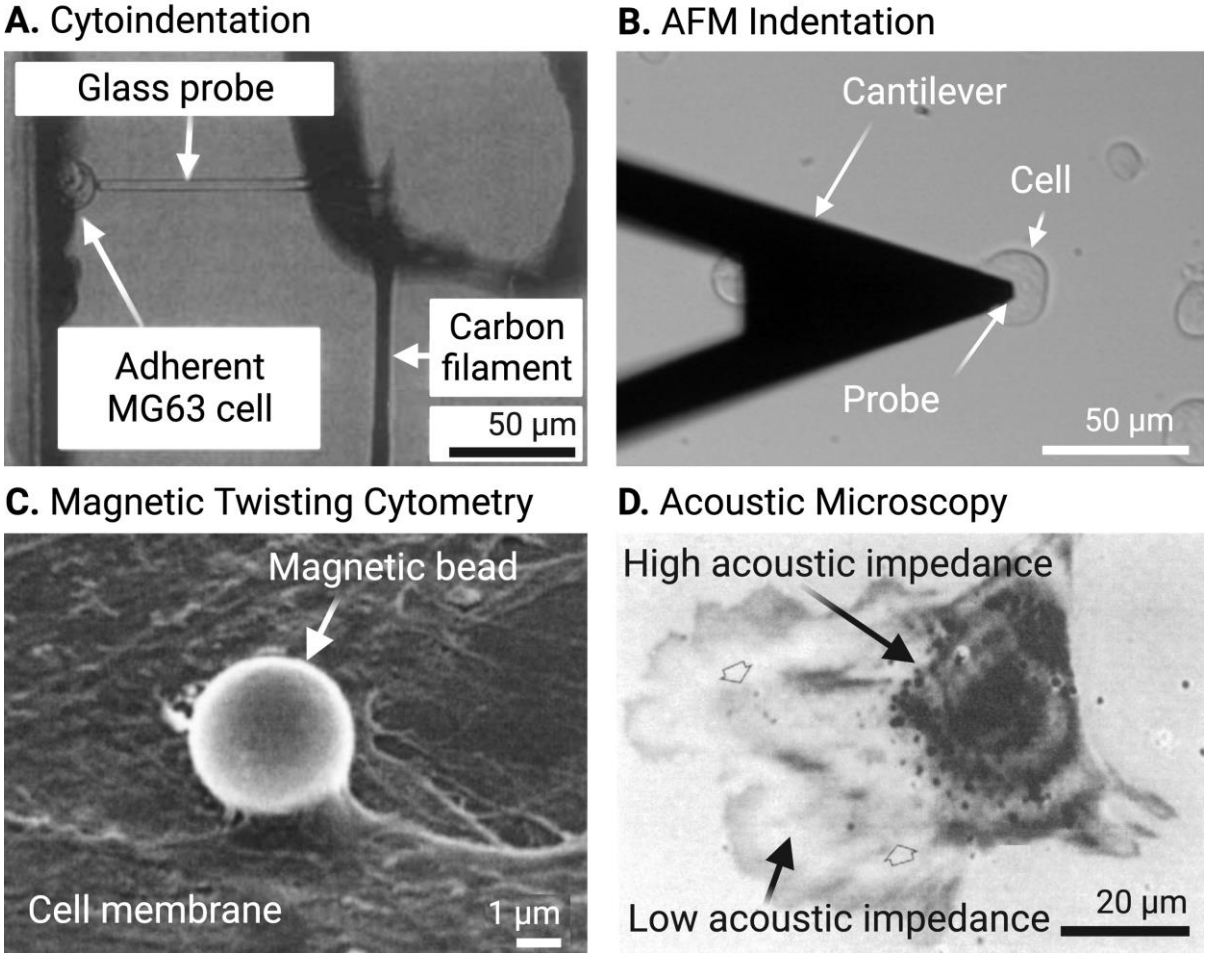

Figure 4. (a) Single MG63 cell compressed under a cytoindenter device consisting of a cantilevered carbon filament and 5 um diameter cylindrical glass probe. Adapted with permission from Shin & Athanasiou (Copyright © 1999 Orthopaedic Research Society).[121] (b) Top view of an ovarian cancer cell under AFM measurement. Adapted from Xu et al.[102] under CC BY 2.0 license (Copyright © 2012 Xu et al.). (c) Scanning electron micrograph of a cell with an adhered magnetic bead for MTC analysis. Adapted with permission from Fabry et al. (Copyright © 2003 American Physical Society).[69] (d) Scanning acoustic micrograph of an adherent cell showing acoustic impedance gradients in the subcellular structure. Regions of high motility appear as comparatively light on the acoustic image, while the trailing features appear darker, corresponding to an increased stiffness-density product. Adapted with permission from Hildebrand et al. (Copyright © 1981 Hildebrand et al.).[122]

Magnetic twisting cytometry

First demonstrated by Crick and Hughes in 1949, Magnetic Twisting Cytometry (MTC) is a mechanotyping method in which cells are probed by small ferromagnetic microbeads under the influence of an applied magnetic field.[30] Here, microbeads are bound to a substrate-adhered cell using a ligand coating (Fig. 4c) and are then magnetised in a specific direction with a strong external magnetic field. A weaker magnetic field is then applied perpendicular to the magnetisation axis, inducing a torque on the microbeads. Analysing the angular displacement of the beads enables a measure of the cellular stiffness at the membrane to be extracted, typically in the form of a shear modulus. An advantage of MTC is the opportunity to apply dynamic loading at a large range of frequencies due to the minimal probe mass, allowing viscous storage and loss moduli to be inferred as well.[31]

MTC has been widely implemented in analysing bulk samples, where aggregate bead rotation data is typically acquired by measuring changes in magnetic flux orthogonal to the "twisting" magnetic field.[31,123,124] As bead rotation causes small linear displacements due to rolling motions, mechanisms have been implemented to track the displacements of individual beads, allowing single-cell membrane stiffness to be locally examined. Such systems measure bead displacement optically,[69,125,126] by laser tracking[32] or using confocal microscopy.[127] MTC applied in this way has enabled detailed frequency-based analysis of the cell membrane, for example finding an inverse response to loading frequency in twisting amplitude for epithelial cells and fibroblasts.[32]

The effective torsional stiffness of each microbead probe is strongly correlated to the contact area between the bead and cell membrane.[123] This, however, limits the reliability of MTC-based measurements of single-cell properties, as the adhesion area may vary significantly between cells.[123] Estimates of the contact area can be obtained, for example by observing actin rings formed at the location of bead adhesion via fluorescent microscopy.[95] However, this is time consuming and only provides approximate results. To date MTC is also limited to use with cells attached to substrates, as a fixed foundation is required to balance the net torque on a cell under MTC analysis. Moreover, as MTC deformability results are dominated by the cell membrane,[32] applications where the stiffness of the cytoskeleton is of interest are less suitable for this technique. This further limits the applicability of MTC in researching and diagnosing diseases for which mechanical biomarkers are related to the actin or microtubule internal structure of cells.[128,129]

Acoustic microscopy

Like electromagnetic waves, propagating acoustic waves experience changes in phase velocity and amplitude during transmission and reflection at material interfaces. These phenomena have been widely exploited to analyse three-dimensional topographies with the advent of technologies such as sonar navigation[130] and medical ultrasound imaging.[131] In these implementations of acoustic imaging, the acoustic contrast at a material boundary is related to the acoustic attenuation of the respective media, and the measured time delay between

transmission and receipt of the acoustic signal is a function of the material's geometry and sound speed.

In 1981 Hildebrand et al. reported the application of a scanning acoustic transducer to capture images of individual cells adhered to substrates with sub-micrometre resolution.[122] Due to variations in density and stiffness within the cell structure, subcellular features are discernible as regions of varied acoustic contrast (Fig. 4d), allowing internal imaging of cell components in a manner analogous to X-ray imaging of the human body. Acoustic microscopy has since been applied to quantitatively characterize the mechanical properties of adherent cells.[132–134] Using modern signal processing techniques, Pasternak et al.[132] measured the height, sound speed, acoustic impedance, density, bulk modulus, and the ultrasonic attenuation properties of MCF-7 cells at different stages in the proliferative, metaphase and apoptotic phases. The authors identified acoustic attenuation as a useful mechanical biomarker, finding marked changes in attenuation at the onset of metaphase and apoptosis. Intriguingly, the presence of two distinct groups within the attenuation distribution for the late apoptotic phase suggests the presence of previously unidentified biological processes and gives further credence to ultrasonic attenuation as a novel mechanical biomarker.

To date, acoustic microscopy of cells has been applied only in scanning scenarios, where an entire cell is imaged, which limits practical sample sizes to hundreds of cells.[132] Single-point measurements equivalent to static AFM indentation, which may improve the throughput of acoustic microscopy for single-cell mechanotyping, have not yet been demonstrated. Additionally, as the reported mechanical properties are sensitive to accurate focusing of the acoustic lens and substrate material selection,[122] the technique is better suited to comparing the mechanical properties of subcellular features than for reporting absolute material constants.

Mechanotyping cells suspended in fluid samples

Optical stretching

Optical stretchers are a group of devices that apply controlled stretching forces to small particles through optical radiation pressure. In this "optical tweezer" approach,[135] the mechanism arises from the change in photon momentum and resultant surface force when passing light through two different refractive media.[136] Consequently, optical radiation forces are dependent on the intensity of incident light and the refractive indices of the particle and medium. By adhering two such particles on either side of a cell, or by passing light directly through a cell, for instance, these can then be positioned in order to apply mechanical forces. In the case of cell stretching, these forces are typically of the order of 100 pN when constrained to using biocompatible optical power levels.[137]

Manipulation of beam geometry enables the design of complex optical pressure fields.[138] Optical tweezer traps require a local minimum in an optical pressure field, which can be generated using two counterpropagating beams[139] or a single converging beam.[140] Both dual-beam and single-beam gradient optical traps have been implemented in mechanical analysis of

cells. Sleep et al. utilised optical tweezers to observe plastic deformation of red blood cell membranes by attaching a pair of glass beads to either side of red blood cell ghosts, each of which was pulled in opposing directions using a single-beam gradient trap[14] (Fig. 5a). The deformation of the cell membrane is observed under a microscope, while the displacement of the beads within each trap enables estimation of the stretching force. Mills et al. subsequently applied this method to whole red blood cells, observing nonlinear elastic and viscoelastic stress-strain properties.[137]

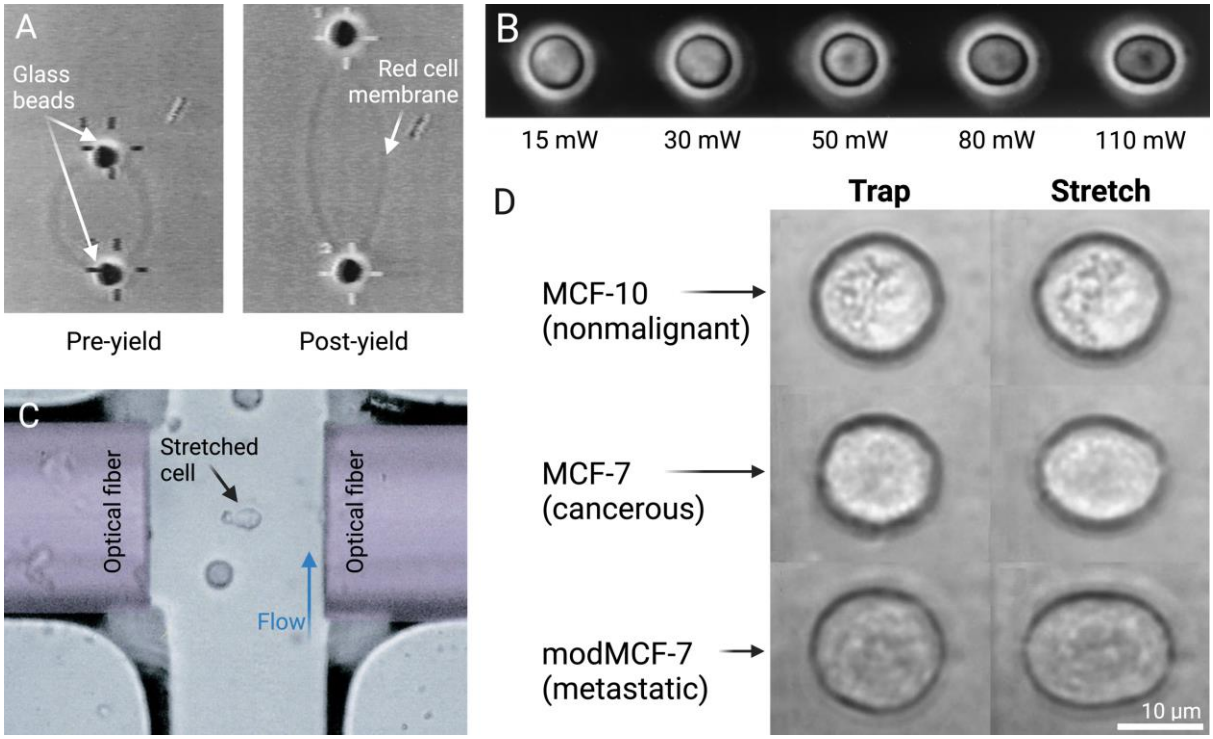

Figure 5. Methods for optical stretch mechanotyping. (a) Plastic behaviour of a red blood cell ghost stretched between two single-beam gradient traps. Adapted with permission from Elsevier (Copyright © 1999 the Biophysical Society).[14] (b) elliptical deformation of a swollen red blood cell with increasing laser power. Reproduced with permission from Elsevier (Copyright © 2001 the Biophysical Society).[60] (c) Top view of a dual-beam microfluidic optical stretcher in operation. Adapted with permission from John Wiley and Sons (Copyright © 2004 Wiley-Liss, Inc.).[33] (d) comparison of optical deformability of three different cell lines: benign MCF-10 cell, malignant MCF-7 cell and modified MCF-7 cell with enhanced metastatic properties. Adapted with permission from Elsevier (Copyright © 2005 the Biophysical Society).[5]

Guck et al.[60] built on this work, using a dual beam "optical stretcher" to exert force directly on the cell surface (Fig. 5b), eliminating much of the manual preparation required for the glass-bead arrangement. They demonstrated the first application of an optical stretcher system in which isolated cells were trapped between two divergent laser beams, similar to the dual-beam traps pioneered by Ashkin et al. in 1970.[139] Unlike the earlier traps, however, the optical

stretcher exploits the nonuniformity of the laser-induced surface normal force to achieve both a stable optical trap and net "stretching" force along the laser axes.

Subsequent work expanded on this technology by incorporating it into a microfluidic system (Fig. 5c), such that individual cells could be temporarily trapped, stretched and analysed at a rate of approximately one cell per minute.[5] This setup was used to probe the mechanical properties of normal and malignantly transformed mouse fibroblasts, as well as human epithelial breast tissue cell lines. Noting the similar refractive indices of the test cells, the authors utilised the observed elliptical ratio of deformed cells at a given laser power as a direct indicator of optical deformability, with tumour cells consistently showing higher deformabilities (Fig. 5d). Similar arrangements have since been used to study a range of cell types and pathological conditions. Remmerbach et al. used an optical stretcher to screen cells from oral carcinomas, finding on average a 3.5-fold increase in deformability and showing good agreement with standard histopathological diagnoses.[7] Agrawal et al. also used an optical stretcher setup to probe links between erythrocyte deformability and Type 2 diabetes, finding a significant reduction in optical deformability in samples from patients with diabetes mellitus and diabetic retinopathy,[10] a complication of the disease causing blindness.[141]

Optical stretcher devices have proven a useful tool for their ability to process free-floating cells in suspension with relatively low experimental labour and good viability of cell samples.[5,7] Moreover, the precise control over the deforming force allows arbitrary strain magnitudes to be applied and enables probing of viscoelastic properties by studying relaxation at step-change loads,[5,7] supporting the use of cell mechanotyping as a label-free biomarker for disease diagnosis.[5,7,10] The throughput, however, of these experimental setups remain well below that required for clinical use, with most optical stretching performed on sample sizes on the order of 10-10^2 cells.[5,7,10] Limitations in achievable throughput are primarily due to the significant creep times observed when deforming cells with weak optical forces,[21] which constrains sequential "trap and release" operations to timescales of the order of 10 seconds.[142] Attempts to improve throughput by deforming cells in slow flows have achieved measurement timescales of the order of 1 second.[142,143] The limited throughput of optical stretching can be attributed primarily to the direct application of optical forces on the cell surface, which while convenient for minimising sample preparation and increasing throughput, also limits stretching forces to the order of 10-100 pN while maintaining cell viability. This constraint arises from the small refractive index difference between cells and common cell media, which dictates that large optical powers (of the order of 1 W) are required to generate nanonewton-scale stretching forces.[5] The reliance of the optical stretching force on optical contrast also introduces a confounding factor when estimating cell stiffness, as observed differences in deformation may be influenced by differences in both stiffness and refractive index.

Dielectrophoretic (DEP) stretching

Dielectrophoretic (DEP) stretching is a process in which a cell is polarised in an AC electrical field and deformed by the resultant dielectric interactions. DEP systems generally consist of one or more electrode pairs submerged in a cell suspension. Applying an AC voltage between the electrodes, often in the 100kHz-10MHz range, causes a nearby cell to be reversibly trapped to one electrode and stretched in the direction of the electrical dipole. First demonstrated in 1984 by Engelhardt et al. using electrodes made from commercial razor blades,[144] the technique has since been integrated into microfluidic systems using conventional microfabrication processes.[44,46,47] DEP stretching applied in this manner has been used to study the viscoelastic properties of red blood cells[144] and cancer cells[44,47] via tuneable and time-sensitive control of the deforming electrical field strength. Due to similarities in the design of non-contact, electronically controlled force fields, DEP stretching represents a convenient and low-cost alternative to optical stretching.[44,46,47] Whereas optical stretching techniques require large laser powers to generate measurable deformations,[5] DEP techniques can achieve similar stretching forces with minimal joule heating.[44–46] DEP systems also benefit from the existence of established photolithographic methods enabling convenient and precise fabrication of embedded electrodes into microfluidic chips, with superior flexibility in achievable force field geometries in comparison to optical stretching systems.[44,46]

Accurate modelling of dielectrophoretic force fields, however, remains challenging due to the complex nature of the electrodynamic interaction between the cell and the electric field. Theoretical and numerical modelling have nevertheless enabled estimation of the equivalent extensional forces acting on cells in a DEP load case.[46,144] However, as with optical stretching, precise calibration of DEP forces is hindered by the involvement of the interplay between dielectric properties of cell components, which are not typically well characterised and may vary between cells and cell types. While previous efforts have compared the results of DEP and comparatively weak optical stretching, direct comparison with other mechanotyping methods at similar strains has yet to be reported. Notably, and in contrast with literature derived from AFM,[108] optical stretching,[5] microfluidic constriction[37] and hydrodynamic[43] approaches, DEP analysis has also shown the apparent stiffness of malignant MCF-7 cells to be significantly greater than those of benign MCF-10A cells.[44] This finding suggests the presence of confounding factors causing variation in the strength of DEP forces that are not present in other mechanotyping analyses.

Micropipette aspiration

As a predominant low-cost technique for probing cell biomechanics, micropipette aspiration devices study cell mechanical properties using a capillary ("micropipette") smaller than the cell diameter. Under a controlled negative pressure, a portion of the cell's volume is sucked into the constriction (Fig. 6a-b), and the protruding distance of the cell membrane ("aspiration length") gives an indication of its relative deformability.

Early implementations of this technique utilised individual micropipettes and micromanipulators to analyse free-floating cells and cells adhered to small beads in suspension. Studies observed both liquid-like[34] and elastic[58] behaviour using this approach. Micropipette

aspiration has since been applied to a wide range of cell types to assess elastic and viscoelastic properties, and is generally considered a gold standard for cell mechanotyping[5,145] due to the fine control over the deforming pressure and the high spatial resolution (250 nm) of deformation measurements.[35] A significant challenge, however, for micropipette aspiration devices is variability in measured stiffness results due to varied aspiration pressures and pipette geometries.[146] Lim et al. presents an explanation for this variability, citing the order of magnitude difference in viscosity of the nucleus and cortex[147] as a potential culprit.[54] In this scenario, the softer cytoplasm will dominate the aspiration process at low pressures, and the much stiffer nucleus will only be deformed (a) if the micropipette aperture is smaller than the nucleus and (b) if the cell is aspirated sufficiently far into the micropipette. Published stiffness results reported using this method are likely confounded by the influence of these subcellular structures due to the simplified continuum models widely used in most analyses.

Another limitation of traditional micropipette aspiration is its very low throughput, which limited to approximately 20 cells per hour.[146] To address this, recent adaptations of the technology have integrated multiple micropipettes into a microfluidic system (Fig. 6c), utilising laminar fluid flow through a contorted channel to generate the aspiration pressure.[38,148–151] This brings multiple advantages over the manual method, with significant improvements in throughput and autonomy, resulting in throughputs of up to 100 cells per hour.[152] A microfluidic design allows for efficient loading of cells into multiple micropipettes for simultaneous measurement without the requirement for manual alignment using micromanipulators.[149] This approach also creates a closed system, eliminating the influence of evaporation.[38] A notable drawback of the microfluidic design, however, is that aspiration pressures are influenced by the trapping state of all pipettes in the array, meaning that efficient trapping is critical to device operation.[151]

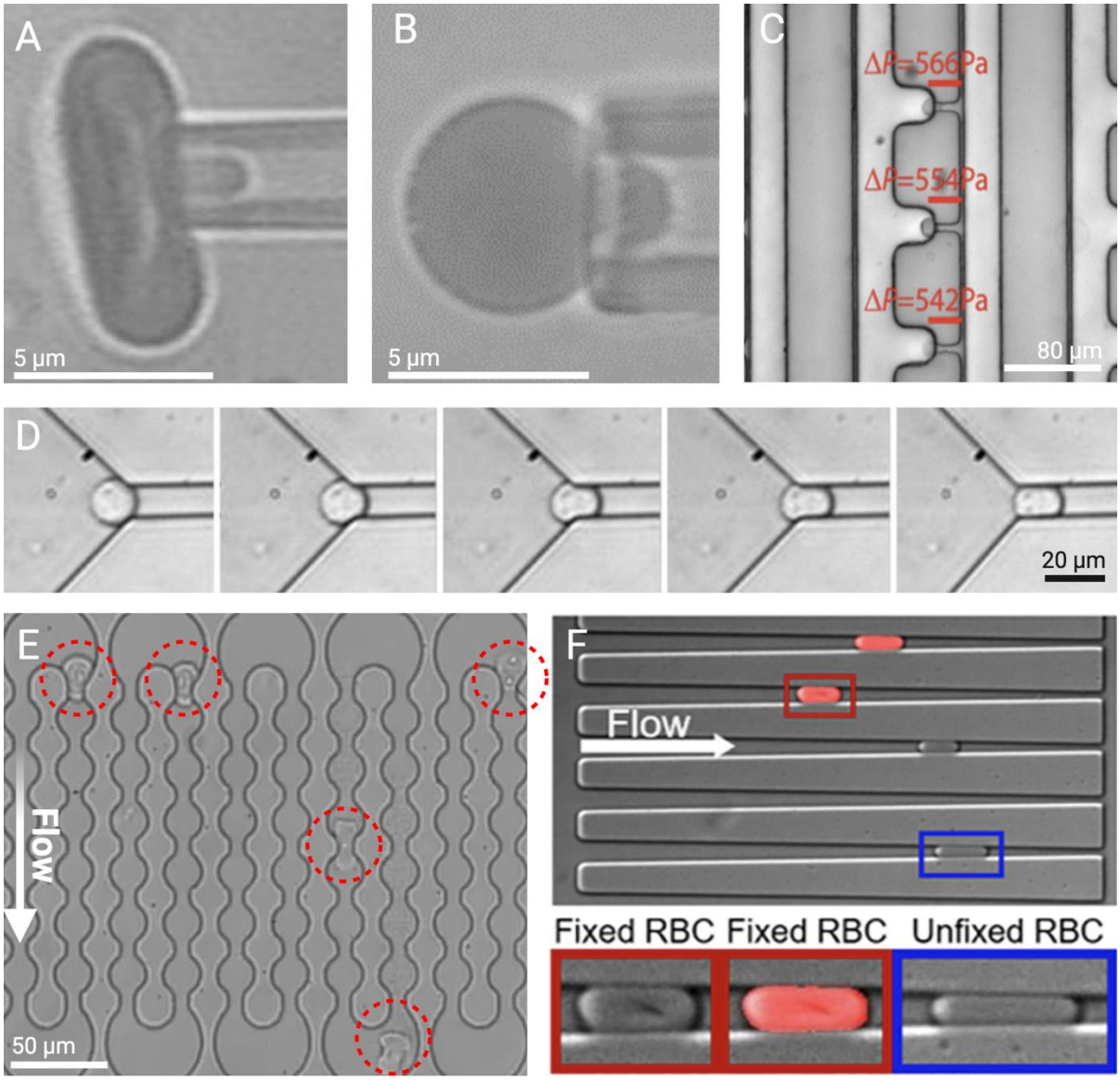

Figure 6. Micropipette aspiration (a-c) and microfluidic constriction transit (d-f) devices. Micropipette aspiration of a bi-concave (a) and swollen (b) red blood cell. Reproduced with permission from Elsevier (Copyright © 1999 Elsevier Science Ltd.).[35] (c) Simultaneous aspiration of single HeLa cells in a microfluidic micropipette aspiration device. Aspiration pressures are shown in red for each micropipette row. Reproduced with permission from Royal Society of Chemistry (Copyright © 2015 The Royal Society of Chemistry).[149] (d) Time series showing entry of a single MCF-7 cell into a 10 µm microfluidic constriction. Reproduced with permission from Springer Nature (Copyright © 2008 Springer Science).[37] (e) Transit of multiple HL60 cells (circled in red) through parallel 5 µm construction arrays. Reproduced with permission from Royal Society of Chemistry (Copyright © 2016 The Royal Society of Chemistry).[56] (f) Comparison of RBC traversal through narrowing channels in a Human Erythrocyte Microchannel Analyser (HEMA) chip. Glutaraldehyde-treated ("fixed") RBCs show a greater resistance to capillary deformation than control ("unfixed") cells. Reproduced with permission from John Wiley and Sons (Copyright © 2020 Navmar et al.).[39]

Microfluidic constrictions

Recently, microfluidic devices have been implemented to assess cells' ability to enter and traverse constrictions smaller than their diameter[37–39,62,145,153] (Fig. 6d). As this process inherently involves large deformations, stiffer cells are more resistant to the constricting forces and generally take longer to squeeze into the smaller channels. An early implementation of this approach was performed by Hou et al. in 2009, in which a low-cost microfluidic device assessed entry time, transit velocity and elongation index of malignant MCF-7 and benign MCF-10A breast cells measured via high-frame rate image analysis.[37] Using this approach, the authors demonstrated a significantly higher entry time for MCF-10A cells than for similarly-sized MCF-7 cells, supporting the consensus that malignant cells generally deform more easily than their benign counterparts.[4–6] This constriction-based approach further mimics the mechanism of cancer metastasis *in vitro,* aiming to replicate the confined geometries and increase in motility through vasculature that is associated with reduced cellular stiffness.[89]

Subsequent work has aimed to improve the reliability and throughput of constriction-based mechanotyping systems. Arraying multiple constrictions in series, for instance, improves the reliability of transit-time measurements by averaging over multiple transit events, while parallel arrays of constriction channels enable simultaneous processing of multiple cells[56] (Fig. 6e). Recent developments in this space have integrated improved cell tracking mechanisms, including embedded electrode pairs for tracking cell transit via electrolytic current,[62,145,153] embedded optical fibres for camera-free optical cell tracking[154] and suspended microchannel resonators (SMRs) to sense cell position along the length of an oscillating cantilever.[155,156] Electrolytic cell tracking systems estimate the projected area of the cell by measuring the increased electrolytic impedance of the microfluidic channel as the cell obscures the fluid volume, allowing estimation of the position along the channel and the instantaneous diameter of the cell. Meanwhile, SMR systems estimate the position of the centre of mass of the cell by analysing changes in the resonant frequency of a MEMS cantilever through which the microfluidic channel runs. By improving the fidelity of cell position measurements and eliminating the need for image analysis, these developments enable throughputs on the order of 10-100 cells per second.[145] Furthermore, these features permit the simultaneous optics-free measurement of additional biophysical characteristics including cellular free diameter, viscoelastic recovery time[145] membrane capacitance, cytoplasmic conductivity[62] and cellular buoyant mass.[155,156]

An inherent limitation of the approach, however, is that measurements of entry time are strongly coupled to cell size.[94] Due to the fixed aperture of the constriction, the degree of deformation required for transversal is heavily dependent on the initial cell diameter and thus is prone to variation with population heterogeneity.[56] This dependency may be partially accounted for by binning cells according to size when collating data[37] or by processing pre-sorted cell groups in different sized constrictions to achieve similar average deformation magnitudes.[145] However, the relationship between cell diameter and transit time is nonlinear, and small variations in cell size may still result in significant measurement noise.[56] Contributing factors to this sensitivity likely include the nonlinear relationship between cell diameter and the constriction wall contact area, and nonlinear stress-strain behaviour in certain cell types.[96] Consequently, a fixed constriction design is unsuitable for comparing cells of

dissimilar size, as different strain magnitudes may yield significant differences in the inferred stiffness. In addressing the significant variability in results from constriction-based techniques, Nyberg et al. also identified reuse of microfluidic constriction devices as a confounding factor due to degradation of internal channel surfaces.[56]

There is also uncertainty as to the dominant mechanical contributor to microchannel transversal behaviour. Nyberg et al. reported that elastic modulus strongly governed transit time in a serial constriction device, with weak influences from particle viscosity and surface tension.[56] Contrastingly, analysis of red blood cells in a modified Human Erythrocyte Microchannel Analyser (HEMA) device[157] showed that the dominant factor driving cell transversal through small channels was their surface area to volume ratio, rather than cell viscoelasticity[39] (Fig. 6f). This discrepancy may be due to different cell types exhibiting solid and liquid-like behaviour, and dominant forces varying between these instances. There is also debate as to whether surface friction has a significant effect on transit time measurements reported using these methods.[37,155] Noting these uncertainties, constriction-based mechanotyping technology would benefit from cross-sectional study to assess the roles of relative cell size, surface properties and material behaviour on the variability of constriction-based stiffness measurements.

Deformability Cytometry: hydrodynamic and inertial stretching

To address the variability of constriction-based mechanotyping, a range of devices have recently been developed utilising fluid flow to generate deforming forces.[40–43,55,57,158–162] This removes the requirement for contact between cells and constriction walls, and greatly reduces the influence of cell size and surface properties on the deformation process.[94] The hydrodynamic mechanism varies between individual devices, which may use combinations of shear flow, extensional flow and inertial effects to deform cells. Broadly, these effects are generated via the use of intersecting microfluidic channels that induce rapid changes in flow direction, converging channel walls that steadily increase flow velocity, or using the natural shear gradient across the width of a narrow channel experiencing Poiseuille flow. In an early implementation of the microfluidic intersection approach, cells are rapidly decelerated at the stagnation point between orthogonally opposed incoming and outgoing flows while being stretched by a combination of inertial and hydrodynamic forces (Fig 7a).[40] Termed "deformability cytometry," this nomenclature has since been adopted by a variety of high-throughput hydrodynamic mechanotyping approaches. This early implementation of the approach produced large cell strains at throughputs of the order of 2,000 cells per second, however the requirement for sequential cell deceleration, deformation and disposal dictates that experimental throughput is limited by inertial timescales as well as the relaxation time of the cell, and therefore has limited capacity for further throughput increases. Moreover, the experimental load case in this regime is not well understood due to the combined influences of fluid shear forces and inertial effects driving cell deformation. Another method utilizing a similar crossed-channel geometry is pinched-flow hydrodynamic stretching, which uses three converging inward flows to create a "hydrolumen" into which the cell is injected[57,158] before being accelerated into a single outlet channel (Fig. 7b). Upon entry into this hydrolumen, transverse converging flows create a pressure gradient across the cell which can be modelled as a drag force acting on the opposing sides of the cell in the directions orthogonal to travel,

while the rapid acceleration of the cell may induce an inertial stretching component in the main flow axis.[57] Due to the absence of sequential cell decelerations, pinched-flow stretching has demonstrated remarkable cell-processing throughputs of up to 65,000 cells per second, though challenges remain in the real-time processing of imaging data at such high throughputs. The pinched-flow approach has also been subject to approximate modelling of deforming forces, which are determined using the combination of a pressure drag force acting on the transverse faces of the cell due to the opposing sheath flow inlets and a viscous drag acting on the cell as it is accelerated by the sheath flow. However, these approximations offer only a first order estimate of the deforming force magnitudes, and do not fully explain the observed experimental results; for example, the inverse relationship between cell size and deformability.[57] The inertial microfluidic cell stretcher (iMCS) approach presented by Deng et al. accelerates cells into collisions with a channel wall at a microfluidic T-junction,[55] upon which cells are inertially compressed in the direction of travel whilst also being subjected to a combination of pressure drag and fluid shear forces (Fig 7c). This approach shares many disadvantages of the extensional flow approach first demonstrated by Gosset et al.; namely, a complex load case and sequentialization of cell decelerations limiting throughput; and as not been widely adopted since publication. However, near real-time image analysis used alongside the iMCS system enabled tracking of the transient effects of single doses of drugs on the deformability of cell populations at moderate throughputs of 100 cells per second, supporting a novel use case for cell mechanotyping in drug testing and development.[55]

An alternative hydrodynamic approach that does not incorporate intersecting channels is real-time deformability cytometry (RT-DC), which exploits fluid shear forces to deform cells into a characteristic "bullet" shape as they pass through a non-contact microfluidic constriction in the Poiseuille flow regime (Fig. 7d). A primary advantage of this arrangement over previous efforts is the lengthened deforming region that increases the deformation timescale for a given throughput, which lowers the minimal required strain rate for measurable cell deformations. The strain rate is further reduced via the addition of methylcellulose to the buffer solution, which increases the fluid viscosity and the strength of the shear forces acting on the cell at a given flow rate.[41] The low strain rate in this regime is critical in minimising the confounding influence of cellular viscosity on cell deformability measurements and has enabled detailed analytical modelling of the hydrodynamic load case for estimation of Young's moduli from RT-DC analyses.[59] Furthermore, the smaller strain rates in this arrangement facilitate on-the-fly quantitative analysis at high throughputs (hundreds of cells per second) owing to reduced image stack size.[13,41] An alternative family of hydrodynamic mechanotyping devices incorporate converging hyperbolic microchannels through which cell suspensions are gradually accelerated as the flow cross section reduces. Here, the hyperbolic channel wall geometry has the unique property of generating extensional flow with constant strain in the direction of travel.[159–163] This characteristic is advantageous in providing an idealised, uniform stress field over the region of observation, as the cell is subjected to a homogenous extensional stretching force while traversing the length of the hyperbolic region.[161] Deviations from this theoretical homogenous force field are evidenced when analysing cell deformation across the length of the hyperbolic region, however as the central region generally provides approximately constant cell deformation these deviations are likely due to edge effects where the hyperbolic region transitions to a straight channel.[161] In part due to the gentle nature of the hyperbolic extensional flow design, hyperbolic channels have been widely used to study red

blood cells at throughputs of the order of hundreds of cells per second, and have not yet been applied for the analysis of stiff tissue cells.

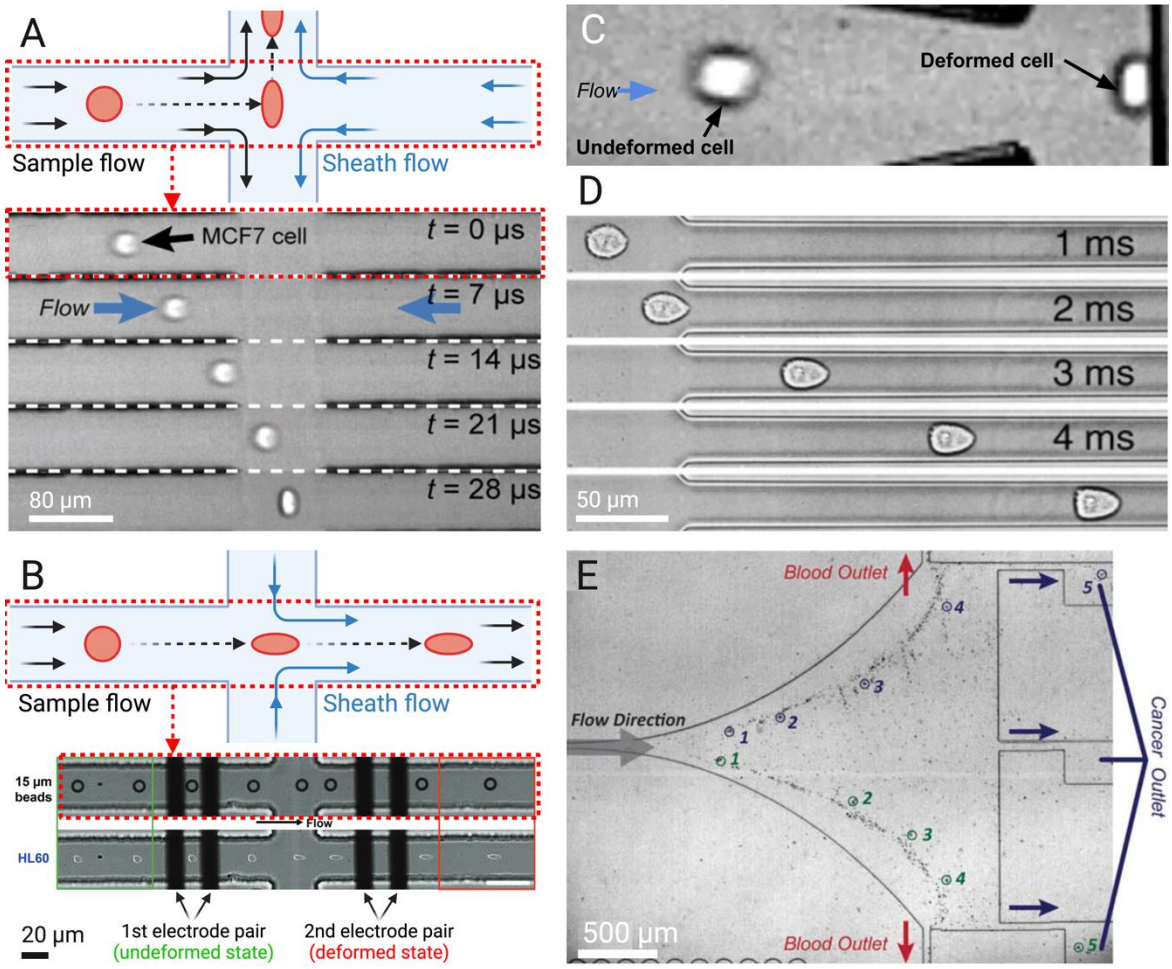

Figure 7. (a) Schematic diagram and time series of an MCF-7 cell in an extensional-flow deformability cytometry device. Adapted from Gosset et al. under PNAS Open Access terms (Copyright © 2012 Gosset et al.).[40] (b) Schematic diagram and time series of a 15um polystyrene bead and HL60 cell in a pinched-flow stretching device. Sequential electrode pairs for optics-free deformation measurement are visible in the experimental micrographs. Adapted with permission from John Wiley and Sons (Copyright © 2022 Wiley-VCH GmbH).[158] (c) Pre- and post-collision geometries of a single MDA-MB-231 cell in the iMCS. Adapted with permission from John Wiley and Sons (Copyright © 2017 John Wiley and Sons, Inc.).[55] (d) Time series of a HL-60 cell in a fluid shear RT-DC device. Reproduced with permission from Springer Nature (Copyright © 2015 Nature America, Inc.).[41] (e) Deformability-activated cell separation via hydrodynamic and inertial lift forces. Red and green annotations highlight individual cancer cells as they migrate away from the streams of red and white blood cells. Reproduced with permission from The Royal Society of Chemistry (Copyright © 2011 The Royal Society of Chemistry).[164]

Deformability cytometry techniques have typically relied on high-framerate imaging and computational image analysis for extraction of quantitative cell deformability distributions. Electrical impedance-based detection methods, however, can also be used for measuring the

position and instantaneous diameter of cells in microfluidic constriction devices.[62,145,153] Recent hydrodynamic approaches have similarly benefitted from the integration of embedded electrodes for optics-free cell deformation measurements.[158,160] This allows optics-free measurement of cell size and deformation under hydrodynamic stretching, either by separately measuring the deformed and undeformed cross sections[158] or simultaneously measuring the minor and major dimensions of the deformed cell via orthogonally-oriented electrode pairs.[160,165] These developments are critical to the accessibility of deformability cytometry as they eliminate the requirements for expensive high-speed imaging and data processing equipment. Electrical impedance methods also bring potential advances in reducing computational and system complexity when processing large cell datasets.

While the specific deforming mechanisms differ between these hydrodynamic and inertial stretching techniques, they each demonstrate high throughputs and large strain magnitudes, produce a distribution of cell deformation measurements against cell diameter, and have demonstrated good cell viability.[40,41,57] These characteristics make deformability cytometry systems promising candidates for clinical use. Tse et al. performed one of the first demonstrations of high-throughput clinical mechanotyping relevance, using a deformability cytometry mechanotyping algorithm to analyse samples from the pleural effusions of 119 patients.[166] This approach was able to diagnose cases of malignancy with 100% positive and negative predictive values in most of the population. Adaptations of deformability cytometry have since been used to perform morpho-rheological analysis of clinical diluted blood samples of patients with leukaemia, and has been proposed as a useful tool for diagnosing malaria.[13]

Deformability cytometry techniques are a promising direction for further development and have many ideal qualities for clinical application, with practical throughputs approaching conventional flow cytometry.[20] Vital to this is the non-contact nature of the deforming force field, which eliminates the influences of substrate stiffness and surface friction that confound cantilever indentation[53] and microfluidic constriction methods.[56] The use of hydrodynamic pressure or shear forces also reduces the dependency of strain on cell diameter by providing a smooth force gradient across the width of the channel, whereas constriction methods rely on the interference between the cell and rigid constriction walls to generate the deforming force.[41,59,94] An overarching limitation of deformability cytometry techniques, however, is that the amplitude of the deforming forces is coupled to the microfluidic flow rate.[40,55,167] This necessitates very short measurement timescales that, while desirable for increasing throughput, inhibit the decoupling of elastic and viscous contributions to measured stiffness.[59] The reliance on microfluidic flow rate to generate deforming force fields also limits the ability to adjust strain magnitudes within a sample, and currently precludes the assessment of nonlinear or dynamic stiffness properties.

Hydrodynamic lift force mechanotyping

Whereas deformability cytometry methods observe the deformation of cells in hydrodynamic force fields, it is also possible to analyse cell properties via comparison of their displacements

due to deformability-induced variations in lift forces. This approach exploits the observation that deformable particles suspended in laminar flows do not strictly follow streamlines, but rather are influenced by a combination of inertial and lift forces that are dependent on their mass and stiffness, respectively.[168] Briefly, the deformability-induced lift force arises from the shape change of an elastic particle in response to hydrodynamic stresses near channel walls in a flowing suspension. The deformed geometry of the particle results in a net lift force when moving relative to the surrounding fluid, for example due to inertial effects or the velocity gradient in Poiseuille flow. As the shape change is aligned to the hydrodynamic stress field the lift force acts perpendicular to flow direction and away from the channel walls. This effect is evidenced by the "tank-treading" behaviour exhibited at high shear rates, in which the cell membrane rotates around the cytoplasm while the ellipsoid geometry of the cell maintains a constant angle of inclination to the flow direction.[169,170] Particles with higher deformability or larger diameters experience a larger contribution due to the exaggerated shape change and larger active surface area, respectively.[171]

The deformability-induced lift force is also a contributing factor to the "cell-free layer" frequently observed near a channel wall in the study of blood flow through small constrictions, and has been proposed as a mechanism driving the shear-thinning behaviour of whole blood.[170] Faivre et al. were among the first to exploit this this phenomenon in a microfluidic chip for plasma separation applications.[171] They also provided early analysis of the effects of particle size, deformability and concentration on the properties of the cell-free layer by comparing healthy, hardened and osmotically swollen red blood cells as well as rigid beads. They found that increased cell deformability consistently led to a larger cell-free layer, indicating an enhancement of the lift force displacing the cells from the channel wall. Due to the short length of the constriction employed, this approach is not effective for single-cell analysis as only the small proportion of cells that are near the channel walls are subjected to significant displacing forces. Recent work, however, has investigated the use of extended channel constrictions[164] and spiral microchannels[172] to achieve inertial sorting of cells according to deformability (Fig 7e). Here, cells migrate to an equilibrium position within the channel where combined inertial forces balance the deformability-induced lift force, with larger and more deformable cells congregating towards the channel centreline, which are then separated into different outlets according to their position within the channel.

The convolution of size and deformability-driven displacements, however, is an inherent limitation to this approach. As the mechanisms driving the deformability-induced lift force are highly nonlinear and not well characterised, manually accounting for the influence of particle size and density to estimate particle stiffness is challenging. Consequently, hydrodynamic lift force mechanotyping has found most utility in cell sorting applications, where quantitative single-cell stiffness measurements are not required. An exception to this trend was recently demonstrated by Maremonti et al., who applied an unsupervised machine learning model to estimate single-cell deformability from the complex dynamic motions of cells in flow.[76] To date this approach has shown proof of concept by identifying the presence of artificial cytoskeletal destabilisation, though work remains to assess its potential for repeatable quantitative deformability measurements.

Acoustofluidic techniques

Whereas hydrodynamic approaches generate forces via shear stresses in continuous flow, acoustofluidic devices utilise acoustic radiation forces to manipulate cells. Here, particles in suspension experience time-averaged forces when subjected to acoustic waves due to nonlinear terms in the Navier-Stokes equations.[173] Surface Acoustic Wave (SAW) and Bulk Acoustic Wave (BAW) devices exploiting this phenomenon have been applied extensively for cell positioning and sorting in microfluidic devices. More recently, acoustic radiation forces have been used to displace or deform suspended cells, giving insight into cellular biophysical properties.[50,52,174]

When the acoustic wavelength is much larger than a particle, acoustic pressure gradients are roughly uniform at the cell scale, and the net acoustic radiation force exerted on the particle can be calculated.[175] This acoustic radiation force is dependent on the acoustic field intensity, position of the particle relative to an acoustic node, the sound speed in the fluid and the acoustic contrast between the particle and fluid materials.[175] In this small-particle regime, the trajectory of a cell in a displacing acoustic field is related to its density and compressibility.[174,176,177] Here, we refer to these devices as “acoustofluidic displacement” mechanotyping technologies. Conversely, when acoustic wavelengths are of a similar size as cell diameter, acoustic pressure gradients can vary significantly across the cell surface. The resultant radiation pressure acting on a cell is thus nonuniform and can produce visible deformations, provided sufficiently large acoustic amplitudes are used.[49] A developing range of “acoustofluidic deformation” mechanotyping devices leverage this effect to assess the viscoelastic properties of cells.[51,52,178,179]

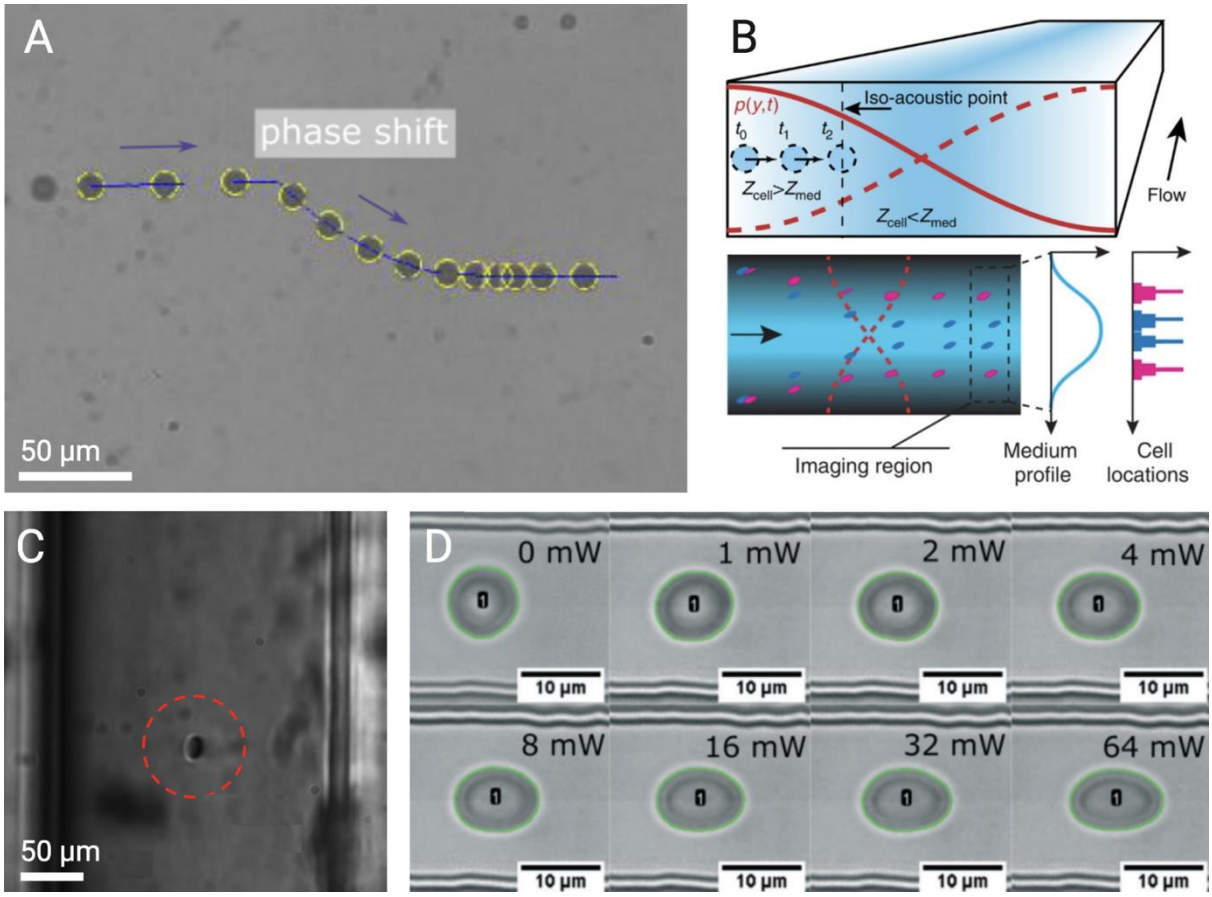

Figure 8. (a) Experimental trajectory of a 10 µm polystyrene bead in a phase-modulated surface acoustic wave device. Reproduced with permission from AIP Publishing (Copyright © 2020 AIP publishing).[150] (b) Schematic representation of the iso-acoustic focussing (IAF) mechanism. The blue gradient visualizes varying acoustic impedance (Z_{med}) throughout the fluid medium. Cells with a given acoustic impedance (Z_{cell}) migrate to positions of zero acoustic contrast where $Z_{cell} = Z_{med}$. Reproduced from Augustsson et al. under CC BY 4.0 license (Copyright © 2016 Augustsson et al.).[176] (c) Acoustofluidic deformations of a swollen red blood cell in a resonant glass capillary. Reproduced with permission from AIP Publishing (Copyright © 2014 AIP Publishing).[49] (d) Acoustofluidic deformation of a bi-concave red blood cell with increasing acoustic power. Reproduced from Link & Franke under CC-BY-NC 3.0 license (Copyright © 2020 Link & Franke).[52]

Acoustofluidic displacement

Acoustofluidic displacement technologies examine cell trajectories in acoustic fields to determine the strength of the acoustic radiation force acting on each cell. Biophysical information can then be inferred by exploiting the dependency of the acoustic radiation force on intrinsic cell properties including density and bulk modulus. To generate these trajectories, cells are first placed at distance away from nodal positions in a stationary acoustic field. This can be achieved by injecting cells near the wall of a microfluidic channel with a half-wavelength resonance condition[50,174] or by shifting the nodes of a SAW field by phase modulation.[150,177] Analysing the response of cells in either scenario gives an indication of their

acoustic contrast in the fluid medium, which can be employed as a comparative biomarker[174] or used to estimate intrinsic properties such as cellular bulk modulus.[177]

Acoustic displacement devices are unique in that displacement measurements are coupled to bulk stiffness, whereas alternative mechanotyping methods measure uniaxial or shear deformation to estimate elastic moduli. The fidelity of this approach, however, is often impeded by the coupling of the net acoustophoretic force on confounding factors, such as cell density and volume.[174] Augustsson et al. reported a novel approach to address this limitation, in which the acoustic impedance of the suspension medium is spatially varied by chemically altering the fluid buffer to achieve size-independent measurements of cellular acoustic impedance.[176] Here, "iso-acoustic focusing" utilises iodixanol, a chemical known to alter the acoustic properties of fluids, to create a stable acoustic impedance gradient in the cell culture medium, with the maximal impedance occurring in the centre of the channel[176,180] (Fig. 8b). Cells located arbitrarily in the channel then migrate to a position of equilibrium where their acoustic impedance equals that of the fluid, termed their "iso-acoustic point". This effectively eliminates the influence of cell volume, addressing a primary reliability issue encountered by Zhao et al.[174] and Wu et al.[177]

While acoustofluidic displacement methods provide a convenient, low-cost method of probing cell mechanical properties, further work is required to assess the suitability of acoustic contrast as a mechanical biomarker. Variations in acoustic impedance (or inferred bulk stiffness) due to artificially induced fixation range from 5-40%, based on a limited number of studies performed with this approach,[150,176,181,182] though less is known about acoustic impedance variations for pathological alteration at a single-cell level. Meanwhile, prior studies probing the uniaxial or shear deformation of cells using other methods have demonstrated changes of 3.5-10 fold[7,33,109,129] with pathological state. While these figures do not provide a direct comparison, they suggest a difference in the sensitivity of bulk and elastic moduli to cytoskeletal alteration, with greater changes in elastic moduli in disease states. Moreover, using acoustic contrast to calculate bulk moduli often relies on the assumption of literature values for cell density,[150,183] which are not widely reported in literature for most cell types. Measurements of bulk modulus obtained using this approach may only be reported within the bounds of the significant uncertainty in these values. Recent work has endeavoured to address this issue using in-situ measurement of cell density to improve the accuracy of bulk modulus measurements.[184,185] These methods estimate cell density by analysing the sedimentation velocity of cells in suspension. However, the weak influence of cell mass makes these measurements challenging,[185] and this approach has not been widely adopted outside of these studies.

Acoustofluidic deformation

Acoustofluidic deformation devices deform cells in suspension by generating large spatial acoustic pressure gradients. Here, deformations are coupled to uniaxial stiffness, which is approximately seven orders of magnitude larger than bulk compressibility[150] and can produce visible strains under microscope analysis.[49,52,179] Mishra et al. first demonstrated the

deformation of osmotically swollen red blood cells in a resonant glass capillary[49] (Fig. 8c). Cells were swollen to a spherical state to eliminate the influence of orientation on the apparent deformation. This limits the applicability of this approach for mechanotyping applications, as the swelling process has confounding effects on measured elastic moduli.[35,186] Acoustofluidic deformation of unswollen red blood cells was first presented by Link & Frank, who described a device capable of simultaneously trapping, orienting and deforming bi-concave red blood cells. The device, denoted the "acoustic erythrocytometer," exploits acoustic diffraction at channel walls to generate a two-dimensional, grid-like pattern of acoustic pressure minima. This acoustic field has the ability to trap cells from continuous flow and induce incremental deformations by varying acoustic power (Fig. 8d). Time-sensitive manipulation of acoustic fields also enables the probing of viscous effects, however, considerable uncertainty in the relaxation time measurements limits the significance of these results.[52] An alternative method of acoustically deforming cells exploits acoustic streaming around a suspended gas bubble in a microfluidic chip.[187] Here, difficulties in modelling the complex acoustophoretic interaction between the bubble and the surrounding cells challenge its use for quantitative analysis, as acoustic streaming field acting on a cell may be significantly altered by the presence of a neighbouring cell. The most heavily researched tool for contactless acoustic cell deformation is the single-beam acoustic tweezer (SBAT). First demonstrated theoretically in 2005,[188] and practically in 2009,[189] SBAT approaches exploit negative acoustic contrast between a particle and its medium or Rayleigh scattering phenomena such that a suspended particle is pulled towards the focal point of an acoustic beam. Noting that cells trapped in the Rayleigh regime also experience compression in the direction of beam propagation, later studies applied this technique for the characterisation of cell deformability by analysing the projected area of a trapped cell in the plane perpendicular to the compression.[77,178,179,190] SBAT devices applied in this way have been used to study cancer cells, finding similar trends of increasing deformability with invasiveness as other techniques,[178,179] while also supporting a novel use case for targeted cancer cell destruction using high acoustic powers.[178] Recent advances in SBAT technology include calibration of deforming forces via comparative micropipette aspiration measurements[178] and the application of a deep learning model to automatically estimate nonlinear elastic moduli of live cells.[77] Collectively, acoustofluidic deformation mechanotyping techniques have been applied to red blood cells,[49,52] breast cancer cells,[77,178] acute lymphoblastic leukemia cells[190] and select tissue cells.[187] . However, each of these studies were restricted to measurement timescales on the order of one minute per cell, and further work is required to prove its efficacy in a high-throughput regime. Nevertheless, demonstrations of fine, time-sensitive control over deforming forces and the suggested scalability to high throughputs[49,52] highlight the technique as a promising contact-free mechanotyping method for clinical use.

Machine learning techniques for single-cell mechanotyping

The potential for machine learning techniques to advance single-cell mechanotyping technology has recently been proposed, namely as a complimentary data analysis tool utilizing any number of cell deformation techniques, [76–79,191,192] or as a standalone system capable of estimating cell deformability via associated morphological features, free from any form of

mechanical probing.[80] Such machine learning approaches offer a methodology for characterising intrinsic cell stiffness properties, which is otherwise complicated owing to the complex biophysical nature and interplay between cellular components, as well as difficulties in calibration and standardization of mechanotyping load cases. Machine learning tools are thus useful in characterising mechanical phenotypes where the relationship between cell stiffness and raw experimental data is nonlinear, noisy or otherwise complex. Machine learning algorithms applied in this manner have accordingly been trained to classify mechanotypes using complex cell trajectories under deformability-induced lift forces,[76] laser diffraction patterns under fluid shear forces,[79] optical images from RT-DC analysis[191] and acoustofluidic deformation forces.[77,192]

The potential for machine learning techniques to identify mechanical characteristics from optical analysis alone has also been investigated.[80] Here, a convolutional neural network was trained on brightfield images of single cells, with reference deformability data generated using a microfluidic "ratchet" constriction device. While the model demonstrated effective prediction of RBC deformability measured using the microfluidic device, the authors do not propose candidate deformability-associated optical markers driving their model. Further investigation is thus required to assess the robustness of these predictions, particularly in discounting the influence of correlated factors such as cell size. This is especially pertinent given that microfluidic constriction technologies (such as the device used to train the model) have widely demonstrated strong correlation between observed deformability and cell diameter.[56,94] The validity of such an approach would thus be greatly supported by comparing model predictions with additional mechanotyping techniques, e.g. AFM indentation or deformability cytometry.

Mechanical models

Having introduced various mechanotyping techniques, here we compare these in Table 1, as well as the mathematical models that are used to relate experimental observations to quantified mechanical properties in Table 2.

Table 1. Comparison of current mechanotyping techniques

Method	Cell sample	Probed domain	Measured variable	Inferred mechanical properties	Clinical demonstration	Reported throughput
Cantilever indentation	Substrate-adhered	Whole cell, Cell surface	Probe displacement	Young's modulus,[64,84] Storage / loss moduli[25]	Yes[6,26,84]	20 minute^{-1} [112]
Magnetic twisting cytometry	Substrate-adhered	Cell surface	Probe angular displacement	Storage/loss moduli[31,32,68,69]	No	100 hour^{-1} [32]
Acoustic Microscopy	Substrate-adhered	Whole cell, subcellular components	Acoustic impedance	Sound speed,[132,133] Acoustic impedance,[122,132,133] Density,[132,133] Bulk modulus,[132,133]	No	10 hour^{-1} [133]

				Acoustic attenuation[132,133]		
Optical stretching	Suspension	Whole cell	Aspect ratio	Young's modulus[60]	No	1 min^{-1} [5]
DEP Stretching	Suspension	Whole cell	Aspect ratio		No	1 min^{-1} [47,48]
Micropipette aspiration	Suspension	Whole cell, Cell surface	Aspect ratio	Young's modulus,[35,58] Cortical tension[34]	No	1 s^{-1} [149]
Microchannel constriction	Suspension	Whole cell	Transit time	Young's modulus*,[148] Cortical tension[62]	Yes[193]	500 s^{-1} [194]
Deformability cytometry	Suspension	Whole cell	Aspect ratio	Young's modulus[59]	Yes[13,166]	65,000 s^{-1} [57]
Hydrodynamic lift force mechanotyping	Suspension	Whole cell	Cell displacement	N/A	No	22,000 min^{-1} [164]
Acoustofluidic displacement	Suspension	Whole cell	Cell displacement	Acoustic impedance,[176] Bulk compressibility[150,177]	No	1000 s^{-1} [174]
Acoustofluidic deformation	Suspension	Whole cell	Aspect ratio, Relaxation time	Young's modulus[77] **	No	1 min^{-1} [52]

*Estimated via comparison with finite element modelling (FEM)

**Estimated via comparison with calibrated hydrogel samples

Table 2. Comparison of common theoretical models for mechanotyping applications

Material model	Independent material parameters	Applied models	Applied to	Conditions of validity
Linear elastic solid	Young's modulus, E Poisson ratio, v	Hertz model[66]	Cantilever indentation[6,8,9,101–103]	Small indentations Probe size << cell radius Probe placement near cell centre Low strain rates
		Elastic half space model[58]	Micropipette aspiration[58]	Small aspiration depth Aperture << cell radius Aspiration depth < aperture Negligible viscousity
		Mietke et al.[59]	Real-time deformability cytometry[59]	Negligible cell viscosity
		Guck et al.[60]	Optical stretching[60]	Small deformations (<10% strain)
Linear viscoelastic solid	Viscoelastic moduli, $k1, k2$ Dynamic viscosity, μ	Viscoelastic Hertz model	Cantilever indentation[27,104]	Small indentations Probe size << cell radius Probe placement near cell centre
		Viscoelastic half space model[67]	Micropipette aspiration[61]	Small aspiration depth Aperture << cell radius Aspiration depth < aperture
Liquid drop	Cortical tension, Tc, (Dynamic viscosity, μ)	Cortical-shell liquid core model[34]	Optical stretching Micropipette aspiration[34,35,100] Microfluidic constriction[62]	Small displacements Negligible influence of cellular substructure
Structural damping	Storage modulus, $G'(\omega)$ Loss modulus, $G''(\omega)$ Poisson ratio, v	Power-Law Hertz model[25]	Cantilever indentation[25]	Small indentations Probe size << cell radius Probe placement near cell centre
		Power-law bead contact model[68]	Magnetic twisting cytometry[31,68,69]	Small displacements Contact patch accurately known
Hyperelastic (Mooney-Rivlin, two parameter)	MR constants, C_{10}, C_{01} Bulk modulus, K	FEM comparison	Cantilever indentation[98]	
Hyperelastic (Neo-Hookean)	Lamé parameters, λ, μ	FEM comparison	Cantilever indentation[195,196] Microfluidic constriction[148] Deformability cytometry[196]	
Acoustophoretic displacement	Bulk compressibility, β	Large-wavelength acoustophoretic model[175]	Acoustofluidic displacement[50,63,150,174]	Cell volume and density accurately known Acoustic field intensity accurately calibrated

Simplified mechanical models drive variability in reported stiffness measurements

Having examined different cell-scale mechanotyping approaches, it is important to note that appropriate theoretical models are required to translate any observed deformations into

quantified mechanical properties. Whereas relatively simple mechanical models are relatively easy to implement, it is commonly reported that measurements of cell stiffness vary with loading conditions, including strain magnitude and direction[98,99,137,147,197] strain rate,[25,31,69,95] probe size[95] and probe location.[53,97] A more comprehensive model of cell mechanics would capture these dependencies, and thus consistently describe the mechanical response of a given cell under a range of relevant load cases. However, the bulk of stiffness measurements reported in mechanotyping studies utilise simplified linear elastic,[6,9,18,58,109,149,150] viscoelastic[4,25,27,67] or Newtonian liquid drop[14,19,34,36] models, each of which neglect many of the aforementioned factors. Here, we provide a brief summary of these and some alternative models, listed in Table 2, and state the assumptions that govern their applicability to various loading scenarios.

Linear elastic models

In cases where strains are sufficiently small, infinitesimal strain theory permits the assumption that the original and deformed coordinate systems are approximately identical, enabling linearisation of the stress-strain relationship. This is characterised by the Hooke's Law relationship $\tau_{ij} = G_{ij}\gamma_{ij}$, where τ_{ij} is the shear stress, G_{ij}, is the shear modulus and γ_{ij} the shear strain in a particular direction given by ij. Often, the isotropic form of this model is used and may be given in the form $\sigma = E\varepsilon$, where σ denotes uniaxial stress, ε uniaxial strain and the Young's modulus $E = 2(1+\nu)G$ for ν the Poisson ratio.[54] Stiff cells or cells undergoing small deformations are often modelled as homogenous elastic solids under this regime, often with the assumption of incompressibility ($\nu \to 0.5$).

Common implementations of this theory include the Hertz[66] and Sneddon[198] models widely used to estimate Young's modulus from cell indentation measurements, which approximate the cell-probe interaction as the indentation of an elastic infinite half space by a rigid cylinder, pyramid, cone or paraboloid.[199] Table 3 summarises common analytical force-displacement relationships for each of these model variants using linear Hertzian analysis, expressed in terms of Young's modulus, for a given indentation depth δ. Here, R is the radius of the cylindrical punch, α is the angle from vertical of the conical or pyramidal faces, and k determines the curvature of the parabolic revolved surface. These approximations become inaccurate (a) at large strains (where nonlinear material behaviour and variations in the contact area become significant),[98] and (b) with misalignment between the probe and cell centre, which causes deviation from the theoretical contact geometry.[53] The assumption of perfectly elastic behaviour also neglects viscous losses, and thus is only valid at low strain rates.[54]

Table 3. Force-displacement relations for common Hertzian models

Probe	**Square pyramid**[200]	**Cone**[198]	**Cylindrical punch**[198]	**Paraboloid**[198]
Force	$F = \frac{1.4906 \tan \alpha}{2(1-\nu^2)} E \delta^2$	$F = \frac{2 \tan \alpha}{\pi(1-\nu^2)} E \delta^2$	$F = \frac{2R}{1-\nu^2} E \delta$	$F = \frac{4\sqrt{2k}}{3(1-\nu^2)} E \delta^{3/2}$

Micropipette aspiration analysis of stiff cells often employs the elastic half-space model, which treats the aspirated portion of the cell as an elastic spherical cap and the portion outside of the micropipette as an infinite elastic volume, yielding the following relationship[58]

$$\Delta P = \frac{2\pi}{3} E \frac{L_P}{R_P} \phi \qquad (1)$$

where ΔP is the aspiration pressure, E is the effective Young's modulus of the cell, L_P is the protruding length of the spherical cap into the micropipette, R_P is the micropipette radius and ϕ is a geometric constant. This analysis effectively neglects any boundary effects outside the micropipette under the assumption that the initial diameter of the cell is significantly larger than the micropipette aperture.[58] However, this simplification loses validity when comparatively large micropipettes are used or where significant aspiration of the cell reduces the excluded volume of the cell.

An alternative analytical model presented by Mietke et al. combines solid elastic theory with the Stokes equation to solve for the deformed geometries of cells undergoing deformability cytometry.[59] Using a first-order perturbation expansion of the stress field acting on the cell surface under Poiseuille flow (i.e. neglecting the influence of the deformed cell shape on the surrounding flow field), the model accurately predicts the characteristic "bullet" shape of cells passing through the non-contact constriction, as well as the relationship between cell diameter and deformation magnitude for a given channel radius. While the model presents good agreement with AFM results for agar calibration samples, reported cellular Young's modulus values are an order of magnitude higher than corresponding AFM measurements. The authors attribute this discrepancy to the short timescale of deformability cytometry measurements in comparison to AFM, which implies that the assumption of steady-state conditions and neglection of cellular viscosity may not be valid at the high strain rates for the HL60 cells used in that study.

Viscoelastic and structural damping models

Variations of the elastic model combine viscous damping effects with linear elastic theory. The linear viscoelastic model permits characterisation of stress relaxation and creep behaviour by introducing a time-dependant term in the linear elastic constitutive equation[67]

$$\tau_{ij} + \frac{\mu}{k_2} \dot{\tau}_{ij} = k_1 \gamma_{ij} + \mu \left(1 + \frac{k_1}{k_2}\right) \dot{\gamma}_{ij} \qquad (2)$$

where k_1 and k_2 are elastic moduli (approximately equivalent to shear moduli) and μ represents the strength of the viscoelastic damping component. In this regime, the characteristic time for relaxation or creep behaviour under transient loading is given by

$$\tau = \mu \frac{k_1 + k_2}{k_1 k_2}. \quad (3)$$

The structural damping model, meanwhile, treats stress and strain as complex quantities, enabling characterisation of the phase relationship between oscillatory stress and strain under frequency-based loading.[201] The mechanical response of the cell is captured in the complex shear modulus $G* = G' + iG''$, where the storage modulus, G', and loss modulus, G'', are associated with elastic deformation and viscous damping respectively. Studies have repeatedly found that $G*$ varies with oscillation frequency, ω, according to a weak power-law relationship.[25,31,69,110]

The viscoelastic and structural damping material models have both been integrated into Hertzian and bead-contact models for cell mechanotyping analysis. To date, these models have been measured using frequency-based AFM[25] and MTC[31,68,69] analysis to characterise the dependence of observed stiffness on the rate or frequency of applied strain. Both the viscoelastic and structural damping models share the same limitations as elastic models in neglecting material and nonlinearity and variation in contact geometry during loading, and consequently their validity is limited to small deformations.

The Newtonian liquid-drop model

Soft cells or cells dominated by membrane stiffness (for example, neutrophils and red blood cells) are commonly modelled as liquid drops.[34,35,39] The liquid drop model characterises a cell's stiffness by its resistance to changes in surface area, reporting a cortical tension (equivalent to the surface tension of a liquid droplet) to characterise its stiffness. This cortical tension was calculated by Evans and Yeung by measuring the critical pressure at which a liquid-like cell was sucked completely into the pipette, and applying the Young-Laplace equation[34]

$$\Delta P_c = 2T_c \left(\frac{1}{R_P} - \frac{1}{R_C}\right) \quad (4)$$

where ΔP_c is the applied pressure differential, T_c is the cortical tension and R_P and R_C are the radii of the micropipette and cell respectively. Often, the viscosity of the theoretical fluid is included in analysis for characterisation of the dynamic response during relaxation or creep events.[35] The liquid drop model inherently neglects any internal cytoskeletal contributions, and therefore acts as a limiting case for cells with a low influence of actin, microtubule or other sub-cellular structures.

Hyperelastic models

Whereas the linear elastic material model is governed by the assumption of infinitesimal strains, hyperelastic models treat the undeformed and deformed geometries as two separate coordinate systems and derive the stress-strain relationship from a strain energy density function under the finite strain theory. This approach gives the unique ability to model large strains and geometric nonlinearity in materials that maintain elasticity at large deformations.[202,203] Recent work supports the application of hyperelastic models in characterising the stress-strain properties of cells, where they have demonstrated agreement over wider experimental strain ranges than linear elastic theory. The neo-Hookean model characterises the elastic response of a material using the Lamé parameters λ and μ, where μ is equivalent to the linear elastic shear modulus G and λ relates to bulk stiffness according to $K = \lambda + \frac{2}{3}\mu$. Despite having only two-independant material parameters, the neo-Hookean model can maintain validity at large strains for some materials.[98] The three-parameter Mooney-Rivlin model gives a more general solution in which the parameters C_{10} and C_{01} define the slope and curvature of the shear stress-strain curve and K is the bulk modulus. To date, hyperelastic modelling has only been applied to cells via comparison with finite element solutions.[98,148,195,196]

Acoustophoretic model

Acoustofluidic displacement mechanotyping techniques are unique in that they do not directly observe cell deformation, instead inferring biophysical information from the displacement interaction between a cell and an acoustic field. In cases where this approach is used to estimate intrinsic mechanical properties, an accurate model of the acoustophoretic force is required. For a small particle in a 1D standing acoustic field in aligned in the x-axis, the net acoustophoretic force is given by[175,164]

$$F_y = \frac{-1}{2\lambda}\pi\, p^2 V_p\, \beta_m\, \phi(\beta,\rho)\, sin(2ky) \quad (5)$$

$$\phi(\beta,\rho) = \frac{5\rho_p - 2\rho_m}{2\rho_p + \rho_m} - \frac{\beta_p}{\beta_m} \quad (6)$$

where λ is the wavelength, p the acoustic pressure amplitude, V_p is the volume of the cell, $\beta_{p,m}$ are the compressibilities of the cell and medium respectively, $\rho_{p,m}$ are the densities of the cell and medium, respectively, k is the acoustic wavenumber and x is the displacement from the nearest acoustic node in the x-direction.

Combining this model with linear elastic theory enables estimation of the bulk compressibility of a whole cell, however this requires calibration of the acoustic field intensity, estimation of cell volume, generally approximated from cell diameter, and assumption of literature values for fluid sound speed and cell density. The resultant uncertainty, combined with the comparatively small influence of cytoskeletal alteration on bulk modulus,[7,84,150] limits the suitability of resulting bulk stiffness as a mechanical biomarker.

Discussion

Proposed applications for single-cell mechanotyping in literature can be broadly classified into two groups, namely; research studies aimed at probing previously unseen mechanical responses in cells, for example with age, disease or the presence of novel therapeutics; and technologies targeting widespread use in clinical environments, where stiffness biomarkers may be leveraged to screen for or diagnose diseases with minimal invasiveness. The distinction between these two applications is significant as each application brings different technical requirements. In the research environment, standardisation of results remains a significant barrier to widespread use of mechanotyping data, where presently reported cell stiffness values vary significantly with the use of alternative mechanotyping techniques.[95] We highlight a general overreliance on simplified mechanical theory as a shortcoming of previous work, particularly in cases where only a small portion of the complete stress-strain relationship is experimentally observed, for example with stiff cells modelled as elastic or viscoelastic solids.

Meanwhile, a clinically useful mechanotyping device should ideally be able to survey a liquid biopsy, generate a distribution of stiffness properties for the sample population, and then output a predictive metric for a disease state with minimal human input. Here, the primary challenge lies in improving the robustness of single-cell stiffness measurements such that the output provides a meaningful indicator, whilst maintaining levels of automation and speed sufficient for processing clinically relevant sample sizes. Here, the most promising technologies are based on deformability cytometry approaches, which combine non-contact force fields in microfluidic flow with high-speed imaging to achieve high throughputs. Current limitations and potential avenues for further work are discussed below.

Mechanical model choice is critical

Surveying the limitations of prevalent mechanotyping models, it is apparent that each is limited to a subset of experimental conditions, and becomes increasingly inaccurate with the confounding influences of nonlinear material stiffness,[98] geometric nonlinearity,[97,204] viscous effects[59,95] or cellular heterogeneity.[53,97] Consequently, commonly reported cell stiffness properties such as Young's modulus and cortical tension have limited significance without a detailed understanding of the experimental setup and specific loading scenario used in each experiment. The significant variation in reported stiffness values for commonly studied cell types is likely due, in part, to difficulties in maintaining appropriate experimental conditions for the corresponding theoretical models.[95] The mechanism driving this variability is two-fold; firstly, finite error is introduced with any deviation from the idealised theoretical load case, and acceptable limits for this deviation are not always maintained. Secondly, limiting experimental setups to the range of loading scenarios where a simplified model is valid often involves sampling a small subset of the available data, which may exclude the range in which mechanical markers of interest are clearly discernible. This also increases the influence of experimental noise, for limiting the measurement range to small strains (and therefore small applied forces) increases the relative strength of confounding factors such as adhesion, subcellular heterogeneity, electrostatic interaction and surface tension.[97,204,205]

Cellular mechanotyping would therefore benefit from the widespread application of more complete mathematical models that characterise cellular properties over a greater range of loading scenarios. In the case of stiff, elastic cells, this may be achieved by abandoning infinitesimal deformation theory in favour of the finite deformation regime. Using a hyperelastic Mooney-Rivlin model, Muller et al. recently demonstrated dramatically increased accuracy over Hertzian analysis for large-strain cantilever indentation of mouse fibroblasts.[98] However, the complexity of large-strain indentation models currently precludes widespread application to mechanotyping experiments in a manner equivalent to Hertzian analysis, and work to date has relied on manual curve fitting with finite element simulation results. A significant obstacle here is the calculation of the instantaneous contact area, which at large deformations is highly nonlinear and varies with the probe shape, depth of indentation, and the relative sizes of the cell and probe.[205] This problem can be partially simplified by treating the cell as a flat, infinite half space and the probe as a sphere, or vice versa; in either case, the contact area becomes dependent only on the depth of indentation relative to the spherical radius. The former approximation has limited utility when attempting to model large cell deformations, as indentations are limited to be of the order of probe size, which is assumed to be much smaller than the cell radius. However, where whole-cell stiffness is of interest and cells are approximately spherical, the use of flat probes may permit analytical modelling of large cell compressions with increased accuracy. At the time of publication, analytical models have been reported for large indentations in hyperelastic half-space materials using spherical probes,[204–206] however no analytical model has been reported for flat-probe compression of hyperelastic spheres.

The confounding influence of cellular heterogeneity on observed stiffness properties is more challenging, as cellular substructures vary significantly between cell types. However, this effect may be minimised in two ways, namely by focusing on whole-cell stiffness measurements, which effectively "average" subcellular stiffness fluctuations, or with models that incorporate generalised subcellular components, for example the compound liquid drop[147,207] or biphasic[29,54] models. As well as the application of the detailed constitutive theory, developing more complete descriptions of cellular mechanophenotypes requires advanced experimental apparatus capable of assessing cellular stiffness under multiple loading conditions. Technologies for conveniently probing individual cell stiffness at a range of strain magnitudes, strain rates and length scales will be valuable in informing new models of increased complexity, and quantifying the dependence of instantaneous cell stiffness on these factors. This will be crucial in developing a standardised framework for comparing intrinsic cell stiffness properties between multiple laboratories or experimental setups. Future work should investigate possible avenues for measuring complex cell stiffness in this manner.

Non-contact deformations are critical for high-throughput mechanotyping

Microfluidic approaches are advantageous for high-throughput mechanotyping and have demonstrated three orders of magnitude increase in measurement rate over alternative methods.[40] While microfluidic constriction methods suffer significant measurement variability due to the strong dependence of strain magnitude on cell diameter and the varying influence of

surface friction, hydrodynamic and inertial methods have emerged as promising alternatives by eliminating contact with constriction walls. As well as eliminating the confounding influence of surface friction and viscous fluid drainage stresses[208] on observed stiffness, non-contact force fields permit the design of smooth pressure gradients over the surface of the cell. When compared to the applied force acting on a cell in a rigid-walled channel, stiffness measurements made using such force fields offer much lower sensitivity to differences in cell diameter when analysing polydisperse cell populations.[41] The elongated deforming region in some deformability cytometry approaches also enables deformation to occur over a larger timespan than the imaging period, allowing the cell to relax into its deformed state and minimising the influence of viscoelastic creep on throughput.[41] Perhaps due to these advantages, deformability cytometry is one of few high-throughput mechanotyping methods that have progressed to clinical application, where it has demonstrated rapid disease screening using liquid biopsies.[13,166]

Table 4. Reported single-cell relaxation/creep times

Relaxation/creep time (approx.)	Cell type	Measured by
100ms – 1s	MDCK cells	AFM indentation[209]
400ms	MG63 cells	Cytoindentation
200ms	J77 cells	MTC[210]
200ms	Red blood cell	Optical stretching[137]
8s	MCF-7 cell	Optical stretching[95]
50ms	Red blood cell	Acoustofluidic deformation[52]
3ms	HL60 cells	Deformability cytometry[211]

An inherent limitation of current deformability cytometry approaches, however, is that the deforming forces are coupled to the microfluidic flow rate. This complicates the measurement of stiff cells, as large forces (and hence large microfluidic flow rates) are required to produce measurable deformations, necessitating the use of high-speed imaging equipment and complex image analysis algorithms.[41] Furthermore, the requirement for high microfluidic flow rates complicates the separation of elastic and viscous properties of cells when estimating their intrinsic mechanical properties. Reported viscous time constants for commonly studied cell types are highly variable, however they generally fall in the range from 10 ms to 1 s. Table 4 gives some characteristic relaxation or creep times for a range of mechanotyping technologies and cell types. In the case of deformability cytometry, artificially increasing the viscosity of the buffer solution, for example by adding methylcellulose,[41,59,212,213] allows strain rates to be reduced to the order of 10^3 s^{-1} while maintaining large cell deformations.[213] However, this is still an order of magnitude faster than the cellular relaxation timescales measured with other mechanotyping methods, suggesting that viscous contributions may still influence observed deformability under deformability cytometry analysis. Further evidence for this conclusion is found in analytical modelling performed by Mietke et al., which overestimated the stiffnesses of HL-60 cells undergoing real-time deformability cytometry by an order of magnitude whilst accurately predicting the Young's modulus of hydrogel calibration particles in comparison to AFM. This suggests that, despite the aforementioned efforts to reduce strain rate, the deformed cell geometries were dominated by viscous relaxation rather than elastic modulus.[59] While this

may be addressed by increasing the length of the deforming channel, other studies aiming to analyse stiffer cells, or study cell deformation in more detail, may encounter practical limitations arising from the required microfluidic flow velocities. The relationship between deforming force and flow rate also constrains cells within a heterogeneous population to be measured under identical conditions and precludes the measurement of individual cell stiffness at multiple strain magnitudes. Here we accordingly highlight the potential to combine the continuous-flow design of deformability devices with other non-contact cell probing methods that allow on-the-fly adjustment of force amplitude, for example optical, dielectrophoretic or acoustofluidic deformation. Previously, constraints in the geometries of optical radiation force fields have restricted such devices to operation at low flow rates, limiting throughputs to three orders of magnitude less than those achieved via deformability cytometry.[129,130] This limitation derives from the comparatively small stretching region achievable by the dual-beam design, combined with the finite timescale required to achieve stable deformation due to viscoelastic creep.[143] Further investigation is warranted to discern if a similar approach may be applied utilising acoustofluidic deformation, which has demonstrated enhanced flexibility in the design of force field geometries[214] and permits high-throughputs,[52,215] but to date has only demonstrated on stationary trapped cells.

Conclusion

Cell mechanotyping research has seen considerable growth in the last decade, particularly in the development of systems with increased automation and throughput for processing large cell samples. However, fundamental limitations in each of the prevalent mechanotyping technologies challenge the use of mechanotyping data in theoretical cell models and the widespread adoption of mechanotyping devices in clinical applications. Higher-precision methods including AFM and micropipette aspiration, for instance, are fundamentally limited in throughput and automation, while a lack of standardisation in loading parameters using these techniques has limited the ability to compare results. While approaches leveraging microfluidic constriction contact bring advantages in throughput and cost, the strong influences of cell diameter and surface friction leads to large variability in indicative stiffness measurements, even for a given cell type. Meanwhile, other high throughput techniques such as deformability cytometry extract limited detail in their measurements of cell deformability. Furthermore, a general overreliance on simplified mathematical models in much of the published work, which either fail to accurately capture experimental loading scenarios or limit analysis to a small portion of experimental datasets, also contributes to the large variability generally reported in reported cell stiffness values.

In progressing the state-of-the-art of single-cell mechanotyping, we highlight two promising avenues for further development. Firstly, in addressing the lack of standardisation of cell stiffness measurements in literature, future work should focus on developing robust, automated approaches for fitting more complex and physically relevant models to mechanotyping experiments. This may include shifting away from infinitesimal deformation theory, which narrows the scope of prevalent force-displacement analysis methods. Here we acknowledge

the interdependency between mechanotyping technology and corresponding theoretical models, and the potential to design novel experimental devices that facilitate convenient application of complex mechanical theory rather than developing theoretical models around pre-existing apparatuses. Such considerations may include the use of flat probes for cell compression experiments, which set the minimum feature size of the system to the cell diameter and allow accurate modelling of cell-scale deformations. Moreover, future work should investigate the application of multi-point stiffness measurements and highly parameterised models, with the goal of capturing more mechanical information from each cell.

Noting the strengths of real-time deformability cytometry as an automated and high-throughput cell analysis system, further investigation into microfluidic systems in which non-contact force fields are decoupled from the microfluidic flow rate is warranted, such that the strength of the deforming forces are independent of the motion of individual cells. While high throughputs are generally favoured for clinical applications, current analysis rates on the order of 1,000 cells per second complicates the separation of elastic and viscous contributions to cell deformation. Candidate non-contact probing technologies include optical stretching, acoustofluidic deformation and DEP stretching, each of which have demonstrated utility in mechanically probing cells, but have yet to be implemented at high throughputs (>1 cells/s). The additional ability to modulate deforming forces on-the-fly, if feasible in a high-throughput scenario, might enable the characterisation of nonlinear stiffness and viscoelastic properties in large cell samples, improving the clustering efficiency of a screening device by adding additional detail to each cell measurement. While the field continues to evolve, cell stiffness measurements nevertheless have the potential to become a useful indicator of cell state and a valuable tool in the study of disease and disease treatment, especially if high-throughput approaches yielding detailed biophysical information can be brought to bear.

References

1 M. A. Model, *Cytometry Part A*, 2018, 93, 281–296.
2 M. Godin, A. K. Bryan, T. P. Burg, K. Babcock and S. R. Manalis, *Applied Physics Letters*, 2007, 91, 123121.
3 D. D. Carlo and D. Di Carlo, *Journal of Laboratory Automation*, 2012, 17, 32–42.
4 K. A. Ward, W. I. Li, S. Zimmer and T. Davis, *Biorheology*, 1991, **28**, 301–313.
5 J. Guck, S. Schinkinger, B. Lincoln, F. Wottawah, S. Ebert, M. Romeyke, D. Lenz, H. M. Erickson, R. Ananthakrishnan, D. Mitchell, J. Käs, S. Ulvick and C. Bilby, *Biophys. J.*, 2005, **88**, 3689–3698.
6 S. E. Cross, Y.-S. Jin, J. Tondre, R. Wong, J. Rao and J. K. Gimzewski, *Nanotechnology*, 2008, **19**, 384003.
7 T. W. Remmerbach, F. Wottawah, J. Dietrich, B. Lincoln, C. Wittekind and J. Guck, *Cancer Res.*, 2009, **69**, 1728–1732.
8 K. Hayashi and M. Iwata, *J. Mech. Behav. Biomed. Mater.*, 2015, **49**, 105–111.
9 M. Lekka, M. Fornal, G. Pyka-Fościak, K. Lebed, B. Wizner, T. Grodzicki and J. Styczeń, *Biorheology*, 2005, **42**, 307–317.
10 R. Agrawal, T. Smart, J. Nobre-Cardoso, C. Richards, R. Bhatnagar, A. Tufail, D. Shima, P. H Jones and C. Pavesio, *Sci. Rep.*, 2016, **6**, 15873.
11 S. Suresh, J. Spatz, J. P. Mills, A. Micoulet, M. Dao, C. T. Lim, M. Beil and T. Seufferlein, *Acta Biomater.*, 2005, **1**, 15–30.
12 H. Bow, I. V. Pivkin, M. Diez-Silva, S. J. Goldfless, M. Dao, J. C. Niles, S. Suresh and J. Han, *Lab Chip*, 2011, **11**, 1065–1073.
13 N. Toepfner, C. Herold, O. Otto, P. Rosendahl, A. Jacobi, M. Kräter, J. Stächele, L. Menschner, M. Herbig, L. Ciuffreda, L. Ranford-Cartwright, M. Grzybek, Ü. Coskun, E. Reithuber, G. Garriss, P. Mellroth, B. Henriques-Normark, N. Tregay, M. Suttorp, M. Bornhäuser, E. R. Chilvers, R. Berner and J. Guck, *Elife*, , DOI:10.7554/eLife.29213.
14 J. Sleep, D. Wilson, R. Simmons and W. Gratzer, *Biophys. J.*, 1999, **77**, 3085–3095.
15 G. B. Nash, C. S. Johnson and H. J. Meiselman, *Blood*, 1984, **63**, 73–82.
16 G. Minatchy, L. Romana, G. Francius and M. Romana, *Microscopy and Microanalysis*, 2020, 26, 47–48.
17 M. A. Lizarralde Iragorri, S. El Hoss, V. Brousse, S. D. Lefevre, M. Dussiot, T. Xu, A. R. Ferreira, Y. Lamarre, A. C. Silva Pinto, S. Kashima, C. Lapouméroulie, D. T. Covas, C. Le Van Kim, Y. Colin, J. Elion, O. Français, B. Le Pioufle and W. El Nemer, *Lab Chip*, 2018, **18**, 2975–2984.
18 J. T. Zahn, I. Louban, S. Jungbauer, M. Bissinger, D. Kaufmann, R. Kemkemer and J. P. Spatz, *Small*, 2011, **7**, 1480–1487.
19 M. G. Millholland, R. Chandramohanadas, A. Pizzarro, A. Wehr, H. Shi, C. Darling, C. T. Lim and D. C. Greenbaum, *Mol. Cell. Proteomics*, 2011, **10**, M111.010678.
20 M. Kozminsky and L. L. Sohn, *Biomicrofluidics*, 2020, **14**, 031301.
21 E. M. Darling and D. Di Carlo, *Annu. Rev. Biomed. Eng.*, 2015, **17**, 35–62.
22 S. Silverman, *Cancer*, 1988, 62, 1796–1799.
23 L. Wang, *Sensors*, 2017, 17, 1572.
24 S. S. Birring and M. D. Peake, *Thorax*, 2005, 60, 268–269.
25 J. Alcaraz, L. Buscemi, M. Grabulosa, X. Trepat, B. Fabry, R. Farré and D. Navajas, *Biophys. J.*, 2003, **84**, 2071–2079.
26 W. A. Lam, M. J. Rosenbluth and D. A. Fletcher, *Br. J. Haematol.*, 2008, **142**, 497–501.
27 E. J. Koay, A. C. Shieh and K. A. Athanasiou, *J. Biomech. Eng.*, 2003, **125**, 334–341.
28 N. O. Petersen, W. B. McConnaughey and E. L. Elson, *Proc. Natl. Acad. Sci. U. S. A.*, 1982, **79**, 5327–5331.
29 D. Shin and K. Athanasiou, *J. Orthop. Res.*, 1999, **17**, 880–890.

30 F. H. C. Crick and A. F. W. Hughes, *Experimental Cell Research*, 1950, 1, 37–80.
31 M. Puig-De-Morales, M. Grabulosa, J. Alcaraz, J. Mullol, G. N. Maksym, J. J. Fredberg and D. Navajas, *J. Appl. Physiol.*, 2001, **91**, 1152–1159.
32 G. Massiera, K. M. Van Citters, P. L. Biancaniello and J. C. Crocker, *Biophysical Journal*, 2007, 93, 3703–3713.
33 B. Lincoln, H. M. Erickson, S. Schinkinger, F. Wottawah, D. Mitchell, S. Ulvick, C. Bilby and J. Guck, *Cytometry A*, 2004, **59**, 203–209.
34 E. Evans and A. Yeung, *Biophys. J.*, 1989, **56**, 151–160.
35 R. M. Hochmuth, *J. Biomech.*, 2000, **33**, 15–22.
36 J. R. Henriksen and J. H. Ipsen, *Eur. Phys. J. E Soft Matter*, 2004, **14**, 149–167.
37 H. W. Hou, Q. S. Li, G. Y. H. Lee, A. P. Kumar, C. N. Ong and C. T. Lim, *Biomedical Microdevices*, 2009, 11, 557–564.
38 Q. Guo, S. Park and H. Ma, *Lab Chip*, 2012, **12**, 2687–2695.
39 A. Namvar, A. J. Blanch, M. W. Dixon, O. M. S. Carmo, B. Liu, S. Tiash, O. Looker, D. Andrew, L. Chan, W. Tham, P. V. S. Lee, V. Rajagopal and L. Tilley, *Cellular Microbiology*, 2021, 23.
40 D. R. Gossett, H. T. K. Tse, S. A. Lee, Y. Ying, A. G. Lindgren, O. O. Yang, J. Rao, A. T. Clark and D. Di Carlo, *Proc. Natl. Acad. Sci. U. S. A.*, 2012, **109**, 7630–7635.
41 O. Otto, P. Rosendahl, A. Mietke, S. Golfier, C. Herold, D. Klaue, S. Girardo, S. Pagliara, A. Ekpenyong, A. Jacobi, M. Wobus, N. Töpfner, U. F. Keyser, J. Mansfeld, E. Fischer-Friedrich and J. Guck, *Nat. Methods*, 2015, **12**, 199–202, 4 p following 202.
42 B. Fregin, F. Czerwinski, D. Biedenweg, S. Girardo, S. Gross, K. Aurich and O. Otto, *Nat. Commun.*, 2019, **10**, 415.
43 M. Liang, D. Yang, Y. Zhou, P. Li, J. Zhong and Y. Ai, *Anal. Chem.*, 2021, **93**, 4567–4575.
44 I. Guido, M. S. Jaeger and C. Duschl, *Eur. Biophys. J.*, 2011, **40**, 281–288.
45 A. Menachery and R. Pethig, *IEE Proc. Nanobiotechnol.*, 2005, **152**, 145–149.
46 G. Bai, Y. Li, H. K. Chu, K. Wang, Q. Tan, J. Xiong and D. Sun, *Biomed. Eng. Online*, 2017, **16**, 41.
47 Y. Teng, K. Zhu, C. Xiong and J. Huang, *Anal. Chem.*, 2018, **90**, 8370–8378.
48 I. I. Hosseini, M. Moghimi Zand, A. A. Ebadi and M. Fathipour, *Sci. Rep.*, 2021, **11**, 2341.
49 P. Mishra, M. Hill and P. Glynne-Jones, *Biomicrofluidics*, 2014, **8**, 034109.
50 H. Wang, Z. Liu, D. M. Shin, Z. G. Chen, Y. Cho, Y.-J. Kim and A. Han, *Lab Chip*, 2019, **19**, 387–393.
51 G. T. Silva, L. Tian, A. Franklin, X. Wang, X. Han, S. Mann and B. W. Drinkwater, *Phys Rev E*, 2019, **99**, 063002.
52 A. Link and T. Franke, *Lab Chip*, 2020, **20**, 1991–1998.
53 S. E. Cross, Y.-S. Jin, J. Rao and J. K. Gimzewski, *Nature Nanotechnology*, 2009, 4, 72–73.
54 C. T. Lim, E. H. Zhou and S. T. Quek, *J. Biomech.*, 2006, **39**, 195–216.
55 Y. Deng, S. P. Davis, F. Yang, K. S. Paulsen, M. Kumar, R. Sinnott DeVaux, X. Wang, D. S. Conklin, A. Oberai, J. I. Herschkowitz and A. J. Chung, *Small*, , DOI:10.1002/smll.201700705.
56 K. D. Nyberg, M. B. Scott, S. L. Bruce, A. B. Gopinath, D. Bikos, T. G. Mason, J. W. Kim, H. S. Choi and A. C. Rowat, *Lab Chip*, 2016, **16**, 3330–3339.
57 J. S. Dudani, D. R. Gossett, H. T. K. Tse and D. Di Carlo, *Lab Chip*, 2013, **13**, 3728–3734.
58 D. P. Theret, M. J. Levesque, M. Sato, R. M. Nerem and L. T. Wheeler, *J. Biomech. Eng.*, 1988, **110**, 190–199.

59 A. Mietke, O. Otto, S. Girardo, P. Rosendahl, A. Taubenberger, S. Golfier, E. Ulbricht, S. Aland, J. Guck and E. Fischer-Friedrich, *Biophys. J.*, 2015, **109**, 2023–2036.
60 J. Guck, R. Ananthakrishnan, H. Mahmood, T. J. Moon, C. C. Cunningham and J. Käs, *Biophys. J.*, 2001, **81**, 767–784.
61 M. Sato, D. P. Theret, L. T. Wheeler, N. Ohshima and R. M. Nerem, *J. Biomech. Eng.*, 1990, **112**, 263–268.
62 Y. Liu, K. Wang, X. Sun, D. Chen, J. Wang and J. Chen, *Cytometry A*, 2022, **101**, 434–447.
63 D. Hartono, Y. Liu, P. L. Tan, X. Y. S. Then, L.-Y. L. Yung and K.-M. Lim, *Lab Chip*, 2011, **11**, 4072–4080.
64 I. A. T. Schaap, C. Carrasco, P. J. de Pablo, F. C. MacKintosh and C. F. Schmidt, *Biophys. J.*, 2006, **91**, 1521–1531.
65 W. R. Jones, H. Ping Ting-Beall, G. M. Lee, S. S. Kelley, R. M. Hochmuth and F. Guilak, *Journal of Biomechanics*, 1999, 32, 119–127.
66 H. Hertz, *Journal für die reine und angewandte Mathematik Band 92*, 1882, 156–171.
67 G. W. Schmid-Schönbein, K. L. Sung, H. Tözeren, R. Skalak and S. Chien, *Biophys. J.*, 1981, **36**, 243–256.
68 B. Fabry, G. N. Maksym, J. P. Butler, M. Glogauer, D. Navajas and J. J. Fredberg, *Phys. Rev. Lett.*, 2001, **87**, 148102.
69 B. Fabry, G. N. Maksym, J. P. Butler, M. Glogauer, D. Navajas, N. A. Taback, E. J. Millet and J. J. Fredberg, *Phys. Rev. E Stat. Nonlin. Soft Matter Phys.*, 2003, **68**, 041914.
70 V. D. Djordjević, J. Jarić, B. Fabry, J. J. Fredberg and D. Stamenović, *Ann. Biomed. Eng.*, 2003, **31**, 692–699.
71 J. L. Drury and M. Dembo, *Biophys. J.*, 2001, **81**, 3166–3177.
72 V. Rajagopal, W. R. Holmes and P. V. S. Lee, *Wiley Interdiscip. Rev. Syst. Biol. Med.*, , DOI:10.1002/wsbm.1407.
73 A. Reece, B. Xia, Z. Jiang, B. Noren, R. McBride and J. Oakey, *Curr. Opin. Biotechnol.*, 2016, **40**, 90–96.
74 Y. Chen, K. Guo, L. Jiang, S. Zhu, Z. Ni and N. Xiang, *Talanta*, 2023, **251**, 123815.
75 D. J. Collins, R. O'Rorke, C. Devendran, Z. Ma, J. Han, A. Neild and Y. Ai, *Phys. Rev. Lett.*, 2018, **120**, 074502.
76 M. I. Maremonti, D. Dannhauser, V. Panzetta, P. A. Netti and F. Causa, *Lab Chip*, 2022, **22**, 4871–4881.
77 O.-J. Lee, H. G. Lim, K. K. Shung, J.-T. Kim and H. H. Kim, *Sci. Rep.*, 2022, **12**, 6891.
78 Y. Chen, C. Ni, L. Jiang, Z. Ni and N. Xiang, *Small*, 2023, e2303962.
79 A. Turgut and Ö. Yalçin, *Biorheology*, 2021, **58**, 51–60.
80 E. S. Lamoureux, E. Islamzada, M. V. J. Wiens, K. Matthews, S. P. Duffy and H. Ma, *Lab Chip*, 2021, **22**, 26–39.
81 J. H.-C. Wang and B. P. Thampatty, *Biomech. Model. Mechanobiol.*, 2006, **5**, 1–16.
82 J. M. Northcott, I. S. Dean, J. K. Mouw and V. M. Weaver, *Front Cell Dev Biol*, 2018, **6**, 17.
83 T. Panciera, L. Azzolin, M. Cordenonsi and S. Piccolo, *Nat. Rev. Mol. Cell Biol.*, 2017, **18**, 758–770.
84 S. E. Cross, Y.-S. Jin, J. Rao and J. K. Gimzewski, *Nat. Nanotechnol.*, 2007, **2**, 780–783.
85 A. S. Kashani and M. Packirisamy, *R Soc Open Sci*, 2020, **7**, 200747.
86 S. Kumar and V. M. Weaver, *Cancer Metastasis Rev.*, 2009, **28**, 113–127.
87 V. Swaminathan, K. Mythreye, E. T. O'Brien, A. Berchuck, G. C. Blobe and R. Superfine, *Cancer Res.*, 2011, **71**, 5075–5080.
88 P. Fernández, L. Heymann, A. Ott, N. Aksel and P. A. Pullarkat, *New J. Phys.*, 2007, **9**, 419.

89 T. Bogenrieder and M. Herlyn, *Oncogene*, 2003, **22**, 6524–6536.
90 A. V. Nguyen, K. D. Nyberg, M. B. Scott, A. M. Welsh, A. H. Nguyen, N. Wu, S. V. Hohlbauch, N. A. Geisse, E. A. Gibb, A. G. Robertson, T. R. Donahue and A. C. Rowat, *Integr. Biol.* , 2016, **8**, 1232–1245.
91 M. Aingaran, R. Zhang, S. K. Law, Z. Peng, A. Undisz, E. Meyer, M. Diez-Silva, T. A. Burke, T. Spielmann, C. T. Lim, S. Suresh, M. Dao and M. Marti, *Cell. Microbiol.*, 2012, **14**, 983–993.
92 D. Qi, N. Kaur Gill, C. Santiskulvong, J. Sifuentes, O. Dorigo, J. Rao, B. Taylor-Harding, W. Ruprecht Wiedemeyer and A. C. Rowat, *Sci. Rep.*, 2015, **5**, 17595.
93 A. Surcel, W. P. Ng, H. West-Foyle, Q. Zhu, Y. Ren, L. B. Avery, A. K. Krenc, D. J. Meyers, R. S. Rock, R. A. Anders, C. L. Freel Meyers and D. N. Robinson, *Proc. Natl. Acad. Sci. U. S. A.*, 2015, **112**, 1428–1433.
94 M. Liang, J. Zhong and Y. Ai, *Adv. Healthc. Mater.*, , DOI:10.1002/adhm.202200628.
95 P.-H. Wu, D. R.-B. Aroush, A. Asnacios, W.-C. Chen, M. E. Dokukin, B. L. Doss, P. Durand-Smet, A. Ekpenyong, J. Guck, N. V. Guz, P. A. Janmey, J. S. H. Lee, N. M. Moore, A. Ott, Y.-C. Poh, R. Ros, M. Sander, I. Sokolov, J. R. Staunton, N. Wang, G. Whyte and D. Wirtz, *Nat. Methods*, 2018, **15**, 491–498.
96 P. Fernández and A. Ott, *Phys. Rev. Lett.*, 2008, **100**, 238102.
97 M. Lekka and P. Laidler, *Nat. Nanotechnol.*, 2009, 4, 72; author reply 72-3.
98 S. J. Müller, F. Weigl, C. Bezold, C. Bächer, K. Albrecht and S. Gekle, *Biomech. Model. Mechanobiol.*, 2021, **20**, 509–520.
99 C. Dong, R. Skalak, K. L. Sung, G. W. Schmid-Schönbein and S. Chien, *J. Biomech. Eng.*, 1988, **110**, 27–36.
100 D. Needham and R. M. Hochmuth, *Biophys. J.*, 1992, **61**, 1664–1670.
101 M. Lekka, *Bionanoscience*, 2016, **6**, 65–80.
102 W. Xu, R. Mezencev, B. Kim, L. Wang, J. McDonald and T. Sulchek, *PLoS One*, 2012, **7**, e46609.
103 P. D. Garcia, C. R. Guerrero and R. Garcia, *Nanoscale*, 2020, 12, 9133–9143.
104 O. Thoumine and A. Ott, *J. Cell Sci.*, 1997, **110 (Pt 17)**, 2109–2116.
105 G. Binnig, C. F. Quate and C. Gerber, *Phys. Rev. Lett.*, 1986, **56**, 930–933.
106 D. Rugar and P. Hansma, *Physics Today*, 1990, 43, 23–30.
107 J. Chen, *Interface Focus*, 2014, 4, 20130055.
108 N. Nguyen, Y. Shao, A. Wineman, J. Fu and A. Waas, *Math. Biosci.*, 2016, **277**, 77–88.
109 M. Lekka, P. Laidler, D. Gil, J. Lekki, Z. Stachura and A. Z. Hrynkiewicz, *Eur. Biophys. J.*, 1999, **28**, 312–316.
110 F. M. Hecht, J. Rheinlaender, N. Schierbaum, W. H. Goldmann, B. Fabry and T. E. Schäffer, *Soft Matter*, 2015, **11**, 4584–4591.
111 Y. M. Efremov, A. X. Cartagena-Rivera, A. I. M. Athamneh, D. M. Suter and A. Raman, *Nat. Protoc.*, 2018, **13**, 2200–2216.
112 Z. Wang, L. Liu, Y. Wang, N. Xi, Z. Dong, M. Li and S. Yuan, *J. Lab. Autom.*, 2012, **17**, 443–448.
113 M. Favre, J. Polesel-Maris, T. Overstolz, P. Niedermann, S. Dasen, G. Gruener, R. Ischer, P. Vettiger, M. Liley, H. Heinzelmann and A. Meister, *J. Mol. Recognit.*, 2011, **24**, 446–452.
114 K. Ghosh, Z. Pan, E. Guan, S. Ge, Y. Liu, T. Nakamura, X.-D. Ren, M. Rafailovich and R. A. F. Clark, *Biomaterials*, 2007, **28**, 671–679.
115 M. E. Murray, M. G. Mendez and P. A. Janmey, *Mol. Biol. Cell*, 2014, **25**, 87–94.
116 M. G. Mendez, D. Restle and P. A. Janmey, *Biophys. J.*, 2014, **107**, 314–323.
117 P. D. Garcia and R. Garcia, *Biophys. J.*, 2018, **114**, 2923–2932.
118 N. Gavara and R. S. Chadwick, *Nat. Nanotechnol.*, 2012, **7**, 733–736.

119 E. K. Dimitriadis, F. Horkay, J. Maresca, B. Kachar and R. S. Chadwick, *Biophys. J.*, 2002, **82**, 2798–2810.
120 A. Meister, M. Gabi, P. Behr, P. Studer, J. Vörös, P. Niedermann, J. Bitterli, J. Polesel-Maris, M. Liley, H. Heinzelmann and T. Zambelli, *Nano Lett.*, 2009, **9**, 2501–2507.
121 Y. Feng, G. Ofek, D. S. Choi, J. Wen, J. Hu, H. Zhao, Y. Zu, K. A. Athanasiou and C.-C. Chang, *Prog. Biophys. Mol. Biol.*, 2010, **103**, 148–156.
122 J. A. Hildebrand, D. Rugar, R. N. Johnston and C. F. Quate, *Proc. Natl. Acad. Sci. U. S. A.*, 1981, **78**, 1656–1660.
123 B. Fabry, G. N. Maksym, R. D. Hubmayr, J. P. Butler and J. J. Fredberg, *Journal of Magnetism and Magnetic Materials*, 1999, 194, 120–125.
124 V. M. Laurent, S. Hénon, E. Planus, R. Fodil, M. Balland, D. Isabey and F. Gallet, *J. Biomech. Eng.*, 2002, **124**, 408–421.
125 B. Fabry, G. N. Maksym, S. A. Shore, P. E. Moore, R. A. Panettieri Jr, J. P. Butler and J. J. Fredberg, *J. Appl. Physiol.*, 2001, **91**, 986–994.
126 M. Marinkovic, K. T. Turner, L. Deng, S. Suresh and J. J. Fredberg, *The FASEB Journal*, 2006, 20.
127 Y. Zhang, F. Wei, Y.-C. Poh, Q. Jia, J. Chen, J. Chen, J. Luo, W. Yao, W. Zhou, W. Huang, F. Yang, Y. Zhang and N. Wang, *Nat. Protoc.*, 2017, **12**, 1437–1450.
128 D. Yamazaki, S. Kurisu and T. Takenawa, *Cancer Science*, 2005, 96, 379–386.
129 A. Calzado-Martín, M. Encinar, J. Tamayo, M. Calleja and A. San Paulo, *ACS Nano*, 2016, **10**, 3365–3374.
130 A. Elfes, *Autonomous Robot Vehicles*, 1990, 233–249.
131 P. N. T. Wells, *Phys. Med. Biol.*, 2006, **51**, R83-98.
132 M. M. Pasternak, E. M. Strohm, E. S. L. Berndl and M. C. Kolios, *Cell Cycle*, 2015, 14, 2891–2898.
133 E. Strohm, G. J. Czarnota and M. C. Kolios, *IEEE Trans. Ultrason. Ferroelectr. Freq. Control*, 2010, **57**, 2293–2304.
134 E. C. Weiss, P. Anastasiadis, G. Pilarczyk, R. M. Lemor and P. V. Zinin, *IEEE Trans. Ultrason. Ferroelectr. Freq. Control*, 2007, **54**, 2257–2271.
135 L. Novotny, R. X. Bian and X. Sunney Xie, *Physical Review Letters*, 1997, 79, 645–648.
136 T. A. Nieminen, G. Knöner, N. R. Heckenberg and H. Rubinsztein-Dunlop, *Methods Cell Biol.*, 2007, **82**, 207–236.
137 J. P. Mills, L. Qie, M. Dao, C. T. Lim and S. Suresh, *Mech. Chem. Biosyst.*, 2004, **1**, 169–180.
138 A. Ashkin, *Proc. Natl. Acad. Sci. U. S. A.*, 1997, **94**, 4853–4860.
139 A. Ashkin, *Physical Review Letters*, 1970, 24, 156–159.
140 A. Ashkin, J. M. Dziedzic, J. E. Bjorkholm and S. Chu, *Opt. Lett.*, 1986, **11**, 288.
141 N. Cheung, P. Mitchell and T. Y. Wong, *The Lancet*, 2010, 376, 124–136.
142 M. Gyger, D. Rose, R. Stange, T. Kiessling, M. Zink, B. Fabry and J. A. Käs, *Opt. Express*, 2011, **19**, 19212–19222.
143 E. W. Morawetz, R. Stange, T. R. Kießling, J. Schnauß and J. A. Käs, *Convergent Science Physical Oncology*, 2017, 3, 024004.
144 H. Engelhardt, H. Gaub and E. Sackmann, *Nature*, 1984, **307**, 378–380.
145 J. Kim, S. Han, A. Lei, M. Miyano, J. Bloom, V. Srivastava, M. M. Stampfer, Z. J. Gartner, M. A. LaBarge and L. L. Sohn, *Microsyst Nanoeng*, , DOI:10.1038/micronano.2017.91.
146 B. González-Bermúdez, G. V. Guinea and G. R. Plaza, *Biophys. J.*, 2019, **116**, 587–594.
147 C. Dong, R. Skalak and K. L. Sung, *Biorheology*, 1991, **28**, 557–567.
148 Y. N. Luo, D. Y. Chen, Y. Zhao, C. Wei, X. T. Zhao, W. T. Yue, R. Long, J. B. Wang and J. Chen, *Sensors and Actuators B: Chemical*, 2014, 202, 1183–1189.

149 L. M. Lee and A. P. Liu, *Lab Chip*, 2015, **15**, 264–273.
150 Y. Wu, T. Cheng, Q. Chen, B. Gao, A. G. Stewart and P. V. S. Lee, *Biomicrofluidics*, 2020, 14, 014114.
151 L. M. Lee, J. W. Lee, D. Chase, D. Gebrezgiabhier and A. P. Liu, *Biomicrofluidics*, 2016, **10**, 054105.
152 P. M. Davidson, G. R. Fedorchak, S. Mondésert-Deveraux, E. S. Bell, P. Isermann, D. Aubry, R. Allena and J. Lammerding, *Lab Chip*, 2019, **19**, 3652–3663.
153 A. Adamo, A. Sharei, L. Adamo, B. Lee, S. Mao and K. F. Jensen, *Anal. Chem.*, 2012, **84**, 6438–6443.
154 F. Storti, S. Bonfadini, G. Bondelli, V. Vurro, G. Lanzani and L. Criante, *Biosensors (Basel)*, 2024, **14**, 154.
155 S. Byun, S. Son, D. Amodei, N. Cermak, J. Shaw, J. H. Kang, V. C. Hecht, M. M. Winslow, T. Jacks, P. Mallick and S. R. Manalis, *Proc. Natl. Acad. Sci. U. S. A.*, 2013, **110**, 7580–7585.
156 S. Byun, V. C. Hecht and S. R. Manalis, *Biophys. J.*, 2015, **109**, 1565–1573.
157 S. C. Gifford, M. G. Frank, J. Derganc, C. Gabel, R. H. Austin, T. Yoshida and M. W. Bitensky, *Biophys. J.*, 2003, **84**, 623–633.
158 C. Petchakup, H. Yang, L. Gong, L. He, H. M. Tay, R. Dalan, A. J. Chung, K. H. H. Li and H. W. Hou, *Small*, , DOI:10.1002/smll.202104822.
159 S. S. Lee, Y. Yim, K. H. Ahn and S. J. Lee, *Biomed. Microdevices*, 2009, **11**, 1021–1027.
160 R. Reale, A. De Ninno, T. Nepi, P. Bisegna and F. Caselli, *IEEE Trans. Biomed. Eng.*, 2023, **70**, 565–572.
161 T. Yaginuma, M. S. N. Oliveira, R. Lima, T. Ishikawa and T. Yamaguchi, *Biomicrofluidics*, 2013, **7**, 54110.
162 V. Faustino, R. O. Rodrigues, D. Pinho, E. Costa, A. Santos-Silva, V. Miranda, J. S. Amaral and R. Lima, *Micromachines (Basel)*, 2019, **10**, 645.
163 M. S. N. Oliveira, M. A. Alves, F. T. Pinho and G. H. McKinley, *Exp. Fluids*, 2007, **43**, 437–451.
164 S. C. Hur, N. K. Henderson-MacLennan, E. R. B. McCabe and D. Di Carlo, *Lab Chip*, 2011, **11**, 912–920.
165 M. Shaker, L. Colella, F. Caselli, P. Bisegna and P. Renaud, *Lab Chip*, 2014, **14**, 2548–2555.
166 H. T. K. Tse, D. R. Gossett, Y. S. Moon, M. Masaeli, M. Sohsman, Y. Ying, K. Mislick, R. P. Adams, J. Rao and D. Di Carlo, *Sci. Transl. Med.*, 2013, **5**, 212ra163.
167 O. Otto, P. Rosendahl, A. Mietke, S. Golfier, A. Jacobi, N. Töpfner, C. Herold, D. Klaue, E. Fischer-Friedrich and J. Guck, *Biophysical Journal*, 2015, 108, 140a.
168 C. K. W. Tam and W. A. Hyman, *J. Fluid Mech.*, 1973, **59**, 177–185.
169 T. M. Fischer and R. Korzeniewski, *Biophys. J.*, 2015, **108**, 1352–1360.
170 T. M. Fischer, M. Stöhr-Liesen and H. Schmid-Schönbein, *Science*, 1978, **202**, 894–896.
171 M. Faivre, M. Abkarian, K. Bickraj and H. A. Stone, *Biorheology*, 2006, **43**, 147–159.
172 E. Guzniczak, O. Otto, G. Whyte, N. Willoughby, M. Jimenez and H. Bridle, *Lab Chip*, 2020, **20**, 614–625.
173 M. Settnes and H. Bruus, *Physical Review E*, 2012, 85.
174 W. Zhao, H. Wang, Y. Guo, K. Sun, Z. Cheng and H. Chen, *Microfluidics and Nanofluidics*, 2020, 24.
175 K. Yosioka and Y. Kawasima, *Acta Acustica united with Acustica*, 1955, **5**, 167–173.
176 P. Augustsson, J. T. Karlsen, H.-W. Su, H. Bruus and J. Voldman, *Nat. Commun.*, 2016, **7**, 11556.
177 Y. Wu, A. G. Stewart and P. V. S. Lee, *Biomicrofluidics*, 2019, **13**, 024107.

178 H. G. Lim, H.-C. Liu, C. W. Yoon, H. Jung, M. G. Kim, C. Yoon, H. H. Kim and K. K. Shung, *Microsyst. Nanoeng.*, 2020, **6**, 39.
179 J. Y. Hwang, J. Kim, J. M. Park, C. Lee, H. Jung, J. Lee and K. K. Shung, *Sci. Rep.*, , DOI:10.1038/srep27238.
180 S. Deshmukh, Z. Brzozka, T. Laurell and P. Augustsson, *Lab Chip*, 2014, **14**, 3394–3400.
181 K. W. Cushing, F. Garofalo, C. Magnusson, L. Ekblad, H. Bruus and T. Laurell, *Anal. Chem.*, 2017, **89**, 8917–8923.
182 K. Olofsson, B. Hammarström and M. Wiklund, *Lab Chip*, 2020, **20**, 1981–1990.
183 R. Dubay, E. M. Darling and J. Fiering, *Microsyst. Nanoeng.*, 2023, **9**, 90.
184 V. Bogatyr, A. S. Biebricher, G. Bergamaschi, E. J. G. Peterman and G. J. L. Wuite, *ACS Nanosci. Au*, 2022, **2**, 341–354.
185 L. Bellebon, H. R. Sugier, J. Larghero, J. Peltzer, C. Martinaud, M. Hoyos and J.-L. Aider, *Front. Phys.*, , DOI:10.3389/fphy.2022.921155.
186 M. A. A. Ayee and I. Levitan, *Curr. Top. Membr.*, 2018, **81**, 97–123.
187 Y. Xie, N. Nama, P. Li, Z. Mao, P.-H. Huang, C. Zhao, F. Costanzo and T. J. Huang, *Small*, 2016, **12**, 902–910.
188 J. Lee, K. Ha and K. K. Shung, *J. Acoust. Soc. Am.*, 2005, **117**, 3273–3280.
189 J. Lee, S.-Y. Teh, A. Lee, H. H. Kim, C. Lee and K. K. Shung, *Appl. Phys. Lett.*, 2009, **95**, 73701.
190 H.-C. Liu, E. J. Gang, H. N. Kim, H. G. Lim, H. Jung, R. Chen, H. Abdel-Azim, K. K. Shung and Y.-M. Kim, *Sci. Rep.*, 2018, **8**, 15708.
191 M. Herbig, A. Jacobi, M. Wobus, H. Weidner, A. Mies, M. Kräter, O. Otto, C. Thiede, M.-T. Weickert, K. S. Götze, M. Rauner, L. C. Hofbauer, M. Bornhäuser, J. Guck, M. Ader, U. Platzbecker and E. Balaian, *Sci. Rep.*, 2022, **12**, 870.
192 H. G. Lim, O.-J. Lee, K. K. Shung, J.-T. Kim and H. H. Kim, *Cancers (Basel)*, 2020, **12**, 1212.
193 M. Faivre, C. Renoux, A. Bessaa, L. Da Costa, P. Joly, A. Gauthier and P. Connes, *Front. Physiol.*, 2020, **11**, 576.
194 X. Yang, Z. Chen, J. Miao, L. Cui and W. Guan, *Biosens. Bioelectron.*, 2017, **98**, 408–414.
195 N. Caille, O. Thoumine, Y. Tardy and J.-J. Meister, *J. Biomech.*, 2002, **35**, 177–187.
196 T. Gao, H. H. Hu and P. P. Castañeda, *J. Fluid Mech.*, 2011, **687**, 209–237.
197 C. Dong and R. Skalak, *J. Theor. Biol.*, 1992, **158**, 173–193.
198 I. N. Sneddon, *Int. J. Eng. Sci.*, 1965, **3**, 47–57.
199 E. Dintwa, E. Tijskens and H. Ramon, *Granular Matter*, 2008, **10**, 209–221.
200 G. G. Bilodeau, *J. Appl. Mech.*, 1992, **59**, 519–523.
201 J. D. Ferry, *Viscoelastic Properties of Polymers*, John Wiley & Sons, 1980.
202 M. Mooney, *J. Appl. Phys.*, 1940, **11**, 582–592.
203 R. S. Rivlin, *Philos. Trans. R. Soc. Lond.*, 1948, **240**, 459–490.
204 D. X. Liu, Z. D. Zhang and L. Z. Sun, *J. Mater. Res.*, 2011, **25**, 2197–2202.
205 M.-G. Zhang, Y.-P. Cao, G.-Y. Li and X.-Q. Feng, *Biomech. Model. Mechanobiol.*, 2014, **13**, 1–11.
206 A. E. Giannakopoulos and A. Triantafyllou, *J. Mech. Phys. Solids*, 2007, **55**, 1196–1211.
207 R. M. Hochmuth, H. P. Ting-Beall, B. B. Beaty, D. Needham and R. Tran-Son-Tay, *Biophys. J.*, 1993, **64**, 1596–1601.
208 Y. Wang, C. Dhong and J. Frechette, *Phys. Rev. Lett.*, 2015, **115**, 248302.
209 E. A-Hassan, W. F. Heinz, M. D. Antonik, N. P. D'Costa, S. Nageswaran, C. A. Schoenenberger and J. H. Hoh, *Biophys. J.*, 1998, **74**, 1564–1578.
210 A. R. Bausch, W. Möller and E. Sackmann, *Biophys. J.*, 1999, **76**, 573–579.

211 F. J. Armistead, J. Gala De Pablo, H. Gadêlha, S. A. Peyman and S. D. Evans, *Sci. Rep.*, 2020, **10**, 3254.
212 L. Guillou, J. B. Dahl, J.-M. G. Lin, A. I. Barakat, J. Husson, S. J. Muller and S. Kumar, *Biophys. J.*, 2016, **111**, 2039–2050.
213 F. J. Armistead, J. Gala De Pablo, H. Gadêlha, S. A. Peyman and S. D. Evans, *Biophys. J.*, 2019, **116**, 1127–1135.
214 K. Kolesnik, M. Xu, P. V. S. Lee, V. Rajagopal and D. J. Collins, *Lab Chip*, 2021, **21**, 2837–2856.
215 C. Devendran, K. Choi, J. Han, Y. Ai, A. Neild and D. J. Collins, *Lab Chip*, 2020, **20**, 2674–2688.